Electrochemical Characterization of Precious Metal Braze Alloys Using Potentiodynamic Polarization

A Senior Project
presented to
the Faculty of the Materials Engineering
California Polytechnic State University, San Luis Obispo

In Partial Fulfillment
of the Requirements for the Degree
Bachelor of Science

by
Maxwell Martin, Mason Morgan, Matthew Vance
June, 2014

Abstract

This study aimed to characterize the electrochemical behavior of six precious metal braze alloys by performing potentiodynamic polarization tests (ParStat 2273) based on ASTM Specifications G5 and G59. To determine the extent to which the alloys will contribute to galvanic corrosion in a marine environment (3.5 wt% NaCl), corrosion analysis software was used to produce fitted Tafel lines to determine the open circuit potential, V_{oc}, for each alloy. The V_{oc} values for the alloys were found to be -66.58 mV for Gold ABA, 13.01 mV for Nicoro®, -39.00 mV for Nioro®, 23.4 mV for Palniro-1®, -47.91 mV for Palniro-7®, and -205.16 mV for Silver ABA. These values were compared to industry-standard base materials typically used in brazing processes to determine their compatibility as galvanic couples. Differences in V_{oc} greater than 250 mV within the couple are considered unsuitable for joining without additional galvanic protection. To provide coupling recommendations, 95% confidence intervals were made to estimate each alloy's V_{oc}.

Keywords: Galvanic Corrosion, Brazing, Potentiodynamic Polarization, Electrochemical Potential, Aerospace, Precious Metal, Materials Engineering

Acknowledgments

We would like to thank Christopher Shipley from Aerojet Rocketdyne (Rancho Cordova, Ca) for his sponsorship and support throughout the course of our senior project. In addition, we wish to acknowledge Alan Demmons from Wesgo Metals (Hayward, Ca) for supplying samples that made our project possible. Lastly, we would like to thank Dr. Blair London for his guidance as our senior project advisor.

Table of Contents

Contents

1. INTRODUCTION 1

1.1 Project Synopsis 1

1.2 Technical Background 1

1.2.1 Brazing 1

1.2.2 Galvanic Corrosion 4

1.2.3 Application 8

1.2.4 Testing 11

2. EXPERIMENTAL PROCEDURE 14

2.1 Sample Cleaning 15

2.2 Electrolyte Preparation 15

2.3 Cell Setup 16

2.4 Potentiodynamic Testing 17

2.5 Statistical Analysis and Base Metal Comparison 18

3. RESULTS 18

3.1 Potentiodynamic Polarization 18

3.2 Statistical Analysis 19

4. DISCUSSION 23

4.1 Sources of Variation 23

5. CONCLUSIONS 26

6. REFERENCES 27

Appendix A 29

Appendix B 30

List of Figures

Figure 1. Schematic of the brazing process with the alloy pulled into the joint by capillary action.[1] 1
Figure 2. Schematic of a galvanic cell showing degradation of the zinc anode and deposition of copper ions from solution onto the cathode.[5] 5
Figure 3. Galvanic series of alloys in a 3.5% NaCl solution representing a seawater environment. A saturated calomel electrode is used as a reference voltage.[6] 6
Figure 4. Relative rate of corrosion in a water solution at varying salt concentrations.[11] 8
Figure 5. Cooling tubes brazed to the outer shell of an engine nozzle.[12] 9
Figure 6. Schematic polarization of a galvanic couple of materials M (anode) and N (cathode). Oxidation reactions have positive slopes while reduction reactions have negative slopes.[14] 12
Figure 7. Potentiodynamic polarization plot depicting the corrosion potential, E_{corr}, and various other points of interest.[15] 13
Figure 8. Corrosion cell setup with all electrodes in place. 16
Figure 9. A schematic view of how the resistor was put into series with the sense and working electrodes.[17] 16
Figure 10. Potentiodynamic Polarization curve for a Palniro-7 sample. The voltage range is ± 250 mV from the open circuit potential at the beginning of the test. A Tafel approximation is shown with the resultant E_{corr} and I_{corr} values. 17
Figure 11. a) Eight potentiodynamic polarization curves for the Nicoro braze alloy. Around the corrosion potential value, there is nearly zero difference among the tests. b) Eight potentiodynamic polarization curves for the Palniro-7 braze alloy. This alloy showed the most scatter and there are clear discrepancies between the trials. 18
Figure 12. Box and whisker plots for each of the six braze alloys. 20
Figure 13. Base-braze comparison showing whether or not each braze alloy lies within the 500 mV range of a particular base metal. The green regions in the box represent the confidence intervals and the large blue lines represent the prediction intervals. a) Base metal A–286, a nickel-based superalloy. b) Base Metal Ti–6Al–4V. 20

List of Tables

Table I: Attributes of Alloying Elements in Braze Alloys 4
Table II: Wesgo Metals Braze Alloy Compositions 15
Table III: Ecorr Measurements of Wesgo Metals Braze Foil Samples 19
Table IV: Final Recommendations for Base-Braze Couples 22

1. INTRODUCTION

1.1 Project Synopsis

Aerojet Rocketdyne (Rancho Cordova, Ca) uses precious metal braze alloys as filler material to join components in their rocket systems. The brazing process places two or more dissimilar metals in contact, a situation where galvanic corrosion can occur. Because the rocket systems are stored in sea air, a particularly corrosive environment, the potential for galvanic corrosion between the braze alloys and the base alloy(s) must be quantified. In order to predict the extent of corrosion, corrosion potential (E_{corr}) values can be found for the six precious metal braze alloys Aerojet Rocketdyne has specified: Gold ABA, Nicoro®, Nioro®, Palniro 1®, Palniro 7®, and Silver ABA. Potentiodynamic Polarization tests, an electrochemical measurement, will be used to quantify the corrosion potential of each braze alloy and statistical analysis will be used to compare these alloys to various industry-standard base metals. Final recommendations on base-braze couples will be made based on an aerospace industry specification which states that joined materials cannot have an electrochemical difference of greater than 250 mV.

1.2 Technical Background

1.2.1 Brazing

Brazing is a joining process which uses a filler alloy to produce a strong joint between two metals. The filler alloy melts during the brazing process and flows into the desired joint location through capillary action before solidifying (Figure 1). In contrast to welding, the base metals being joined do not melt during the brazing process. The distinction between soldering and brazing is the processing temperature—an operation which occurs above 450°C is considered brazing while joining at temperatures below 450°C is called soldering.

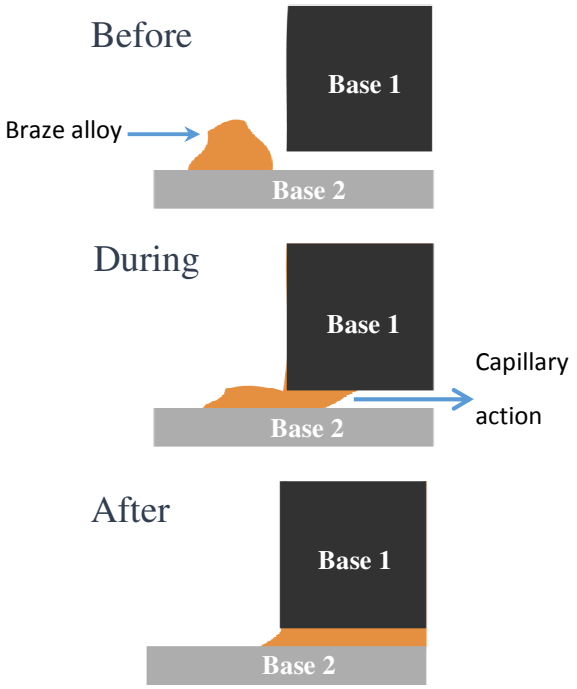

Figure 1. Schematic of the brazing process with the alloy pulled into the joint by capillary action.[1]

Perhaps the most important consideration when selecting a braze alloy is the melting range, specifically the solidus and liquidus temperatures. Heating a material to the solidus temperature causes some phases of the alloy to begin to melt but the entire alloy will not liquefy until the liquidus temperature is reached.[2] For capillary action to occur, the braze alloy needs to be molten. For this reason, most brazing operations will use a heat treatment 20-30°C above the liquidus temperature to ensure proper flow into the joint.[2]

For braze foils, a common as-purchased form, the gap between the two dissimilar base metals does not need to be large; once the braze foil melts, capillary action will allow the metal to flow into a joint as small as the gap resulting from each metal's surface roughness.[1] Capillary action is a phenomenon reliant on the attraction force a liquid has in contact with two closely-fitted surfaces. This ability of a liquid filler metal to pull its mass along the contact surfaces allows for brazing of joints of complex geometry. As the filler alloy begins to solidify, it interacts with each base metal which gives strength to the joint. The braze material will penetrate surface irregularities on the base metal and, in some cases, react with the base metal and form intermetallic products along the interface, a phenomenon which generally provides strength but can be undesirable if these resultant intermetallics are brittle.[2]

Furnace brazing, the technique used by Aerojet Rocketdyne, requires a clean surface, an inert environment, and temperature-controlled cycles. Furnace brazing is ideal for large scale manufacturing due to its repeatability and ease of automation but many factors still affect the properties of the joint. These additional factors include the temperature, time, and pressure of the furnace cycle.[1] Foils in the aerospace industry are often furnace brazed under vacuum conditions. Vacuum furnaces eliminate the oxygen in the atmosphere and reduce the oxidation and oxide formation on the metals during joining, reducing the need for additional flux material. A vacuum furnace secures the part within the chamber and, during heating, rotates the part along its central axis to allow even heat distribution and proper flow of the liquefied

braze alloy. Although furnace brazing is typical of the industry, brazing can also be performed with a torch or through induction heating.

Advantages

The main benefits of brazing are that it is a controllable process and can join dissimilar metals with complex geometries at a high degree of repeatability. In addition, because the melting temperature (T_m) of the braze alloy is considerably less than the T_m of the base metals, the risk of warping and distortion of the base component is minimized.[2] This means that components with widely different thicknesses and cross-sectional areas can be brazed together. Another advantage is that in some specific cases, brazing can be completed during the heat treatment of a component, a technique which increases production rate and maximizes efficiency.

Limitations

Although brazing is an effective joining technique in some applications, it has some unwanted side effects and disadvantages. For one, the filler alloys are costly due to the presence of precious metals, preventing the adoption of brazing in many industries and products. Also, during the brazing process the parts must be held together with a pre-determined spacing or the joint strength may suffer; the gap between the base materials is a significant factor in the overall joint strength upon solidification.[2] In addition, although the base materials do not melt during the operation, they are still subjected to a heat treatment which may result in microstructural changes and, in turn, diminished mechanical properties.

Brazing Alloys

The aerospace industry typically uses precious metal braze alloys for its brazing applications because of their performance advantages; each alloying element adds unique attributes and as a result, manufacturers are able to tailor filler metals for specific applications (Table I).

Table I: Attributes of Alloying Elements in Braze Alloys

Alloying Element	Attributes
Gold[3]	Free from volatiles and has exceptional resistance to oxidation and other types of corrosion at high temperature.
Nickel[1]	High strength and corrosion resistance at high temperature. One disadvantage is that nickel can impede flow in a melt.
Silver[1]	Melting temperature suppressant. Enhances capillary flow and improves corrosion resistance of less-noble alloys.
Copper[1]	Wetting and molten metal flow properties are increased which improves corrosion resistance.
Palladium[3]	Adds corrosion resistance including oxidation resistance at high temperatures. Has higher mechanical strength than gold and does not form brittle intermetallics.
Titanium[3]	Typically used in active braze alloys to wet ceramic materials.

Brazing alloys are available for use in a wide range of forms including rods, wires, pastes, powders, laminates, tapes, and foils.[4] Typically, foils are used in the regeneratively cooled nozzles on rocket engines because they can easily be wrapped around the conical sections being joined. Brazing is utilized for joining circular shapes because the associated capillary action is capable of providing higher joint strength than many other joining techniques.

1.2.2 Galvanic Corrosion

Because the brazing process typically involves joining dissimilar metals, designs using brazed components should carefully consider the electrochemical behavior of each metal to minimize the effects of galvanic corrosion. Galvanic corrosion is a process where one metal corrodes preferentially in the presence of another metal, resulting in a galvanic cell. In order for galvanic corrosion to occur, specific requirements must be met: the two metals must have different electrochemical potentials, be in electrical contact, and be immersed in a common electrolyte (Figure 2).[5] Under these conditions, the dissimilar metals are called a galvanic couple because

one metal, the anode, will undergo oxidation (Equation 1) while the other metal, the cathode, will be reduced (Equation 2). This redox reaction causes the anode to lose electrons to the cathode, resulting in dissolution (corrosion) of the anodic material. This phenomenon is one of the most common forms of corrosion and is a concern in a variety of different industries—everything from international tankers to microelectronic devices must prevent the effects of galvanic corrosion.

$$M \rightarrow M^{n+} + ne^- \quad \textbf{(1)}$$

$$M^{n+} + ne^- \rightarrow M \quad \textbf{(2)}$$

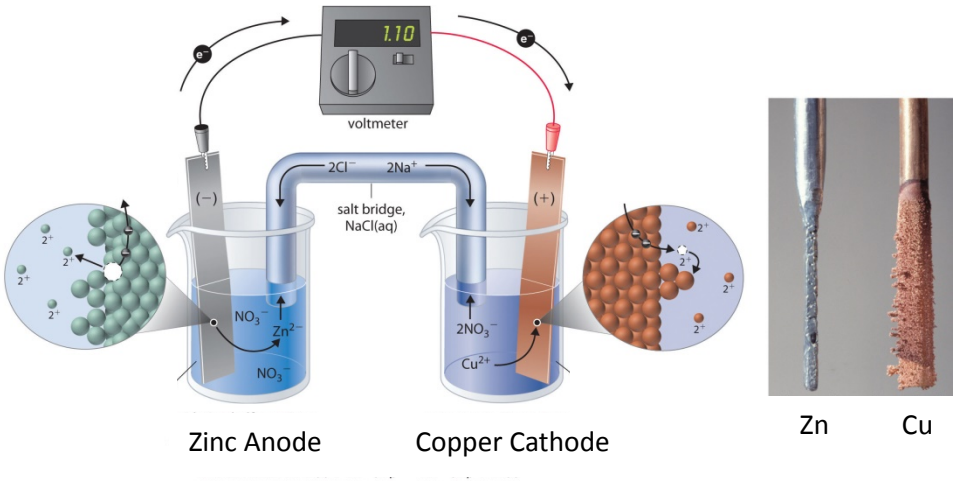

Figure 2. Schematic of a galvanic cell showing degradation of the zinc anode and deposition of copper ions from solution onto the cathode.[5]

Galvanic Series

In order to aid in the design process, electrical potential values for a variety of alloys are tabulated to generate a galvanic series (Figure 3).[6] A galvanic series table is used to determine the order of a group of metals/alloys from anodic (least noble) to cathodic (most noble) in a

specific environment and in reference to a specific electrode.[7] This series can be used to determine the approximate extent of galvanic corrosion when two materials are placed in electrical contact. In theory, a larger difference in potential between two alloys will result in more severe galvanic corrosion because this incongruity in electrochemical potential is the driving force for dissolution.[7] It is of note that each galvanic series is generated in a specific environment as the order can change depending on the electrolyte and temperature. A galvanic series is generated with electromotive force (EMF) values, the force that quantifies the tendency of an alloy to give up electrons in a specific environment.[8] In electrochemical terms, the EMF is the summation of the oxidation potential and the reduction potential in the cell.[9]

Figure 3. Galvanic series of alloys in a 3.5% NaCl solution representing a seawater environment. A saturated calomel electrode is used as a reference voltage.[6]

Galvanic Corrosion Factors

The corrosive effect of the couple is affected by the surface area exposed to the electrolyte and the distance between the two materials. Mixed potential theory states that the current at the anode must be equal to the current at the cathode in a galvanic couple. However, differences in area between the anode and cathode will result in different current densities at these two locations; Faraday's Law states that it is the current density which ultimately controls the galvanic corrosion rate.[10] When the cathodic region is large in comparison to the anodic region, the current density at the anode is increasingly large and increases the corrosion rate dramatically. Since the braze material will have a smaller area than the base metal, it needs to be more cathodic to prevent aggressive corrosion. Also, the distance between the coupled metals affects the corrosion rates—two materials close to one another will undergo galvanic corrosion more quickly than the same two materials far apart. However, with a highly conductive electrolyte like seawater, this distance effect is minimized.[6] In addition to the conductivity of the electrolyte, activity in the galvanic cell also depends on other variables within the environment. The pH of the solution changes the extent of corrosion, with a more acidic environment (low pH) having a greater concentration of H^+ ions dissolved in solution and promoting attack (increasing the corrosion rate of the cell).

Marine Environment

Although technological advances and decades of experience have alleviated many problems, due to the potential for catastrophic failure with rockets, it is important that the flight distance over populated areas is minimized. For this reason, rockets are launched from coastal locations towards the ocean. This launch locale necessitates that large structural components are stored on the coast in a marine environment. These warm coastal locations provide a particularly corrosive electrolyte because highly ionic materials such as Cl^- and SO_4^{2-} are carried by onshore winds. Seawater has a salt concentration of around 3.5% which has been estimated as the most corrosive salt solution (Figure 4).[11]

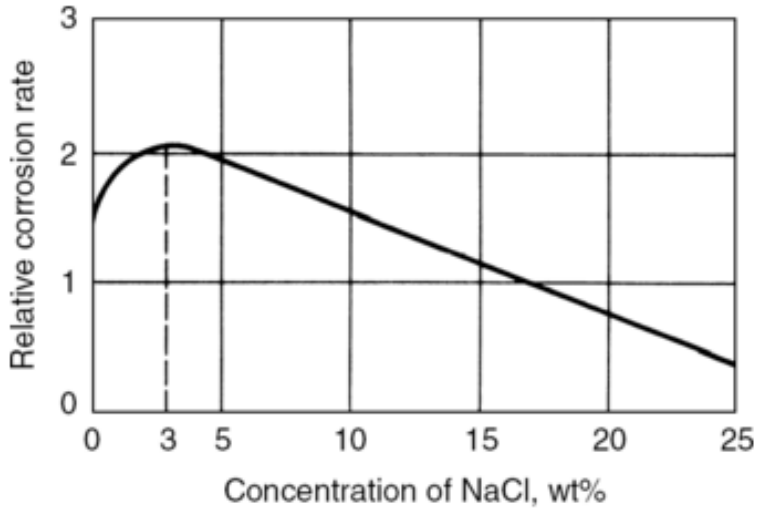

Figure 4. Relative rate of corrosion in a water solution at varying salt concentrations.[11]

Both chloride and sulfate ions contribute to all forms of corrosion, as an increased concentration of ions leads to a more conductive electrolytic solution. In addition, chloride ions are capable of penetrating and breaking down passive films, leading to degradation of previously passive metals like stainless steels. The marine air brings a common electrolyte to the joined parts and sets up galvanic corrosion between the dissimilar metals.[11]

1.2.3 Application

Aerojet Rocketdyne has a long history in the field of rocket propulsion that encompasses solid propellant engines, liquid propellant engines and other components used in rockets and missiles. Of these areas, brazing technology is of particular importance in the fabrication of liquid propellant rocket engines. Some of the major components of the liquid propellant rocket engine that utilize brazing are fuel impellers, thrust chambers, and regeneratively cooled nozzles.

Specific Applications

Nozzle cones are the familiar bell-shaped structures found at the aft end of a spacecraft launch vehicle. The main purpose of these structures is to maximize the thrust obtained by the combustion reaction that occurs inside the thrust chamber. It follows that the interior wall of the nozzle experiences extreme temperature variations pre-flight, during launch, and after main engine shutoff. These variations occur because of the presence of hot, high pressure gases and due to the space environment. During these significant thermal events, especially during the high-temperature period when the engine is ignited, mechanical properties can be impaired resulting in engine failure and eventual spacecraft failure. In order to negate this effect, liquid rocket engines are designed with different types of cooling systems. Primarily, designs involve regenerative and ablative cooling systems. Regenerative cooling involves the movement of fuel through the structure while ablative nozzles remove heat through the loss of material. This removal then exposes a new unheated surface, lowering the overall temperature of the structure. Of concern to Aerojet Rocketdyne and the process of brazing are the regeneratively cooled rocket engines that utilize small pipes or channels that run down the length of nozzle (Figure 5).[12]

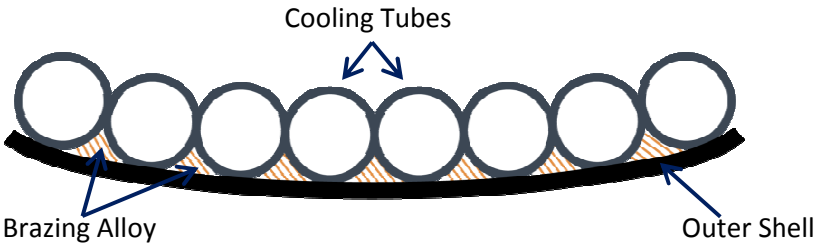

Figure 5. Cooling tubes brazed to the outer shell of an engine nozzle.[12]

With half of the pipes running down from the fuel tanks to the bottom of the nozzle and the other half returning the fuel up to the fuel impeller, the system uses the cryogenic liquid propellant which cools the nozzle before being ignited to generate thrust in the thrust chamber. Because hundreds of pipes are used in the cooling system, welding each pipe is impractical and

could lead to variable joint properties. Through furnace brazing, each pipe/channel can be joined to the nozzle at one time in a temperature-and humidity-controlled chamber.

In addition to regeneratively cooled nozzle cones, many high-pressure applications within rocket engines utilize brazing as their primary joining process. Because these structures are exposed to high velocity gases, pressures can exceed 10,000 psi in certain sections. Although the brazed joints do not carry these loads alone, they must maintain high strengths to avoid failure during their service life. These components are optimal candidates for brazing due to their complex geometries which eliminate many other joining techniques.

Braze Alloys

Precious metal braze alloys are commonly utilized in aerospace applications because the alloys are capable of meeting the stringent property requirements and, compared to other industries, the aerospace industry can afford higher cost materials if they offer a performance benefit – what the industry cannot afford is failure. In general, the design requirements specify a filler metal with high corrosion resistance, high strength at elevated temperatures, fluidity, compatibility with a base metal, and some ductility for vibrations and expansions in service. Alloying elements such as gold, palladium, and silver are relatively inert and limit the extent of corrosion which occurs in operation. These alloys also offer high strength, providing joints with the capability of withstanding the extreme conditions and stress concentrations in service. Precious metal braze alloys also offer good wettability and flow during the brazing process which produces better capillary attraction and improves the quality of the final joint.

1.2.4 Testing

Electrochemical Testing

Although the mechanisms of galvanic corrosion are well understood, quantifying galvanic activity can be a difficult task. Electrochemical testing is commonly used to evaluate corrosion potential and develop a control plan to minimize its negative effects. These tests offer estimations of the component lifetime, assessment of corrosion potential of coupled materials, and insight into the mechanisms and limiting factors of the corrosive reaction. In general, electrochemical experiments are relatively fast (especially when compared to weight loss measurements of corrosion) and are the only way to continuously monitor the corrosion rate over a wide variety of oxidizing conditions.[9]

As mentioned previously, galvanic corrosion occurs when redox reactions bring electrons from one site (anode) and transfer them to another site (cathode). This process results in a corrosive current, a measurable value which is a valuable predictor of the overall corrosion rate. In general, an electrochemical measurement is performed by controlling one or more of the factors in Ohm's Law (V=IR): voltage, current, or resistance.

Testing for galvanic corrosion can be performed using a potentiostat, an instrument capable of monitoring and controlling a circuit to make electrochemical measurements. A standard potentiostat testing setup is comprised of working, reference, and counter electrodes. A potentiostat controls the potential of a test specimen with respect to a reference electrode which contains a metal immersed in an electrolytic solution and has a stable, known electrochemical potential. The way the potentiostat regulates the galvanic cell is through a voltage feedback op-amp which monitors and supplies the current required to maintain the voltage across the working electrode. The potentiostat controls the potential between the reference and working electrodes, finding the applied voltage, known as the V_{cell}, required to make the potentials match. The current that is required to produce V_{cell} is the polarization current. There are two main types of polarization: activation and concentration. In activation

polarization, the corrosion reaction is controlled by the free energy (potential driving force) at the surface of the electrode. Concentration polarization is controlled by the ability of reactants to move through the solution. Due to the high conductivity of salt water, activation polarization is the mechanism which controls the corrosion and a linear trend is seen in the polarization plot. The polarization curves generated by a potentiostat can be used to determine other properties including corrosion rates and corrosion potential values.

In the case of two corroding metals, each with its own specific corrosion potential (E_{corr}), the corrosion potential for the couple (E_{couple}) should be between the anodic and cathodic E_{corr} values (Figure 6).[14]

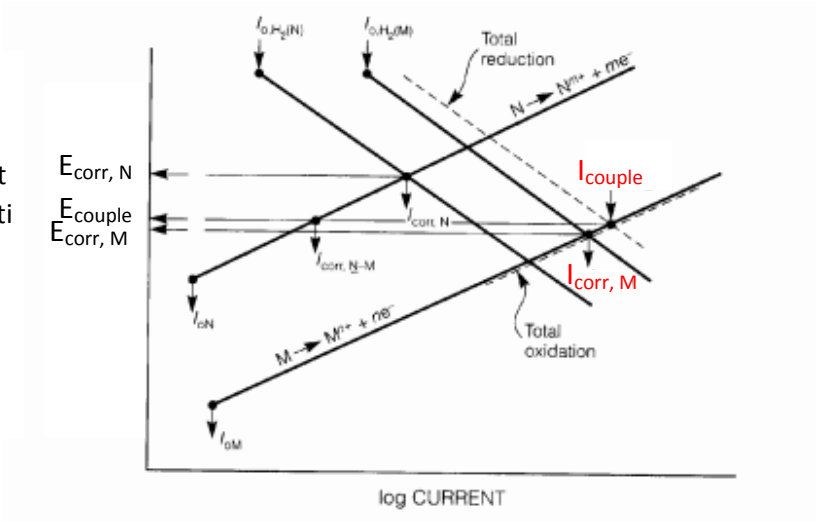

Figure 6. Schematic polarization of a galvanic couple of materials M (anode) and N (cathode). Oxidation reactions have positive slopes while reduction reactions have negative slopes.[14]

In examining the graph, it is apparent that the oxidation current of M increases after being coupled with N because i_{couple} is larger than $i_{corr, M}$. Similarly, it can be seen that the reduction current of N increases due to the pairing. Essentially, material M corrodes but also offers some protection to material N, actually decreasing its overall corrosion rate.

Potentiodynamic Specifics

The tests that are run using the potentiostat are potentiodynamic and will generate polarization curves for each of the alloys. The potentiodynamic test involves a "sweep" in which the potential is increased at a linear rate until an upper limit is reached. During the sweep, the resultant current is monitored and plotted in real time. A typical sweep rate is around 10 mV/minute (0.6 V/hour).[9] However, for each experimental setup the sweep rate should be maximized to find the fastest scanning rate without altering the results (generally accepted practice is changing the data by less than a factor of 2). This optimization allows tests to be performed efficiently without changing the accuracy of the results. Potentiodynamic polarization tests (Figure 7) are useful because computers and software can perform and plot the tests continuously in real-time, a fact which leads to better resolution than related potentiostatic test methods. The generated polarization curve plots the potential in volts against log current. Tafel fit lines are then placed on the graph on both the cathodic and anodic reaction sections; the intersecting point of the two Tafel curves is the open-circuit potential (EMF value).

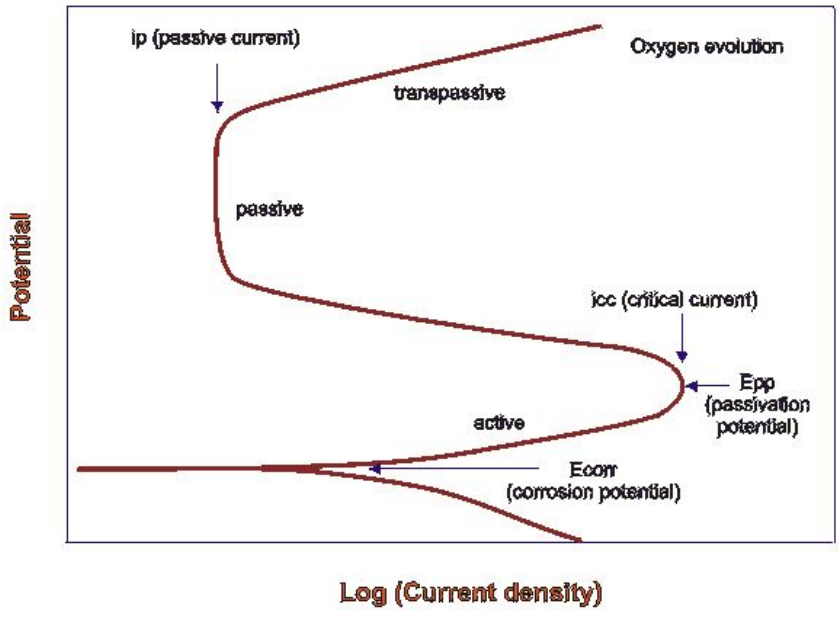

Figure 7. Potentiodynamic polarization plot depicting the corrosion potential, E_{corr}, and various other points of interest.[15]

A typical polarization curve for a passivating material has three distinct regions: active, passive and transpassive.[9] The active region occurs during the beginning of the testing phase where the material is actively corroding. When a critical potential has been reached, the material reaches the passive region and the corrosion rate decreases. The alloy forms a passive layer that inhibits any further corrosion of the specimen and has a stable current until the potential increases to the point where the passive layer is compromised. In the transpassive layer, the sample is again actively corroding until the end of the testing parameters. The transition points or intersections between these regions on the graph correlate to significant electrochemical analysis values. The "nose" between the active and passive sections contains the passivation potential and critical current values that are then used for further calculations. The last nose that occurs between the passive and transpassive sections indicates the location of the passive current.

For our project, the most important value from this plot is the E_{corr} value which represents the approximate EMF value for each braze alloy. This value will be compared against the known EMF values of the base metals and the galvanic corrosion rate will be estimated.

2. EXPERIMENTAL PROCEDURE

A modification of ASTM Standard G5 was used to conduct the potentiodynamic polarization tests for each of the alloys. After results were collected, analysis using statistical software was performed to determine the extent of galvanic corrosion in each base-braze couple. This project had not been conducted at Cal Poly so writing a detailed standard operating procedure was a component of the project (Appendix B).

2.1 Sample Cleaning

The samples used in the testing were thin, circular foils supplied by Wesgo Metals (Hayward, Ca) and measured .625'' in diameter, with a thickness of 0.006'' (Table II).

Table II: Wesgo Metals Braze Alloy Compositions

	Gold ABA	Nicoro®	Nioro®	Palniro-1®	Palniro-7®	Silver ABA
Gold (Au)	**96.4**	**35**	**82**	**50**	**70**	0
Silver (Ag)	0	0	0	0	0	**92.75**
Copper (Cu)	**3**	**62**	0	0	0	**5**
Nickel (Ni)	0	**3**	**18**	**25**	**22**	0
Palladium (Pd)	0	0	0	**25**	**8**	0
Titanium (Ti)	**0.6**	0	0	0	0	**1.25**
Aluminum (Al)	0	0	0	0	0	**1**

*Nominal compositions are in weight percent

Samples were cleaned based on a procedure established in ASTM G5. In accordance with this procedure, samples were placed in a beaker of acetone and submerged in an ultrasonic cleaning bath for two and half minutes. After ultrasonic cleaning, each sample was rinsed with deionized water before being placed in the testing apparatus. Although the ASTM standard calls for a grinding and polishing procedure prior to sample cleaning, this was not feasible for the foil samples because of their thicknesses. Additionally, the cleaning specification suggests using a solution of boiling benzene as the best cleaning medium, but our investigation decided to use acetone for ease of handling and disposal.

2.2 Electrolyte Preparation

The electrolyte chosen for the testing was a 3.56% NaCl solution which mimics sea water.[16] This solution is more corrosive than sea air and should therefore give a worst-case approximation of a coastal environment. To produce the solution, 34.00 ± 0.001 g of Morton's non-iodized salt was added to 920 mL of distilled water and stirred until homogeneous.

2.3 Cell Setup

The electrochemical cell used in this investigation was made up of a working electrode, a reference electrode and a set of counter electrodes (Figure 8). The working electrode is where the sample is located and where the electrochemical measurements are taken during the experiment. The reference electrode, a saturated calomel electrode for this study, has a well-known corrosion potential, and is compared to the measurements taken at the working electrode. The counter electrode serves to complete the electrochemical circuit and stabilize the current passing through the system. A chemically inert conductor is usually used for the counter electrode, with a pair of graphite rods serving this purpose in this study. Each of these electrodes is connected to the potentiostat, with an additional "sense" lead being attached in series with the working electrode. The sense lead is used as a secondary measure of the voltage across the sample. Because no current is passing through the sense lead, there is no ohmic drop and the true potential at the working electrode can be controlled. In addition to the sense lead being added to the system, a resistor is placed in series with the working and sense leads (Figure 9). The resistor is used to filter some of the noise from the results.

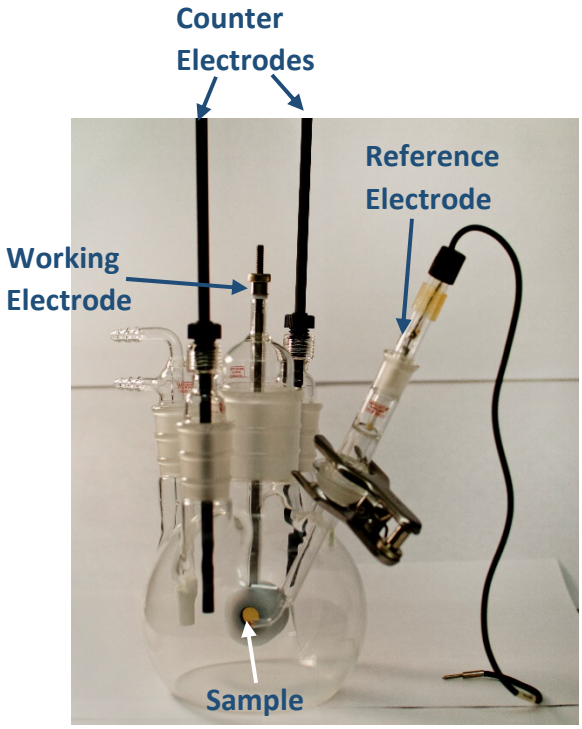

Figure 8. Corrosion cell setup with all electrodes in place.

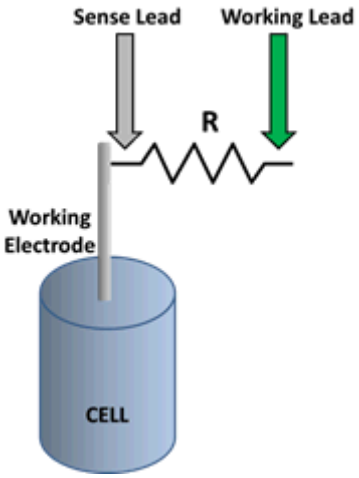

Figure 9. A schematic view of how the resistor was put into series with the sense and working electrodes.[17]

2.4 Potentiodynamic Testing

Once the cell was set up, the salt solution was allowed to equilibrate for approximately 30 minutes. According to Leah Sheridan from Princeton Applied Research, the manufacturer of the potentiostat, an acceptable drift rate was 2-3 mV / minute.[17] The drift was monitored by running an open circuit E_{corr} versus time experiment with the same software. At the beginning of every test, the original open circuit potential was observed to help determine if the test was starting in the correct potential range. Once a drift rate in the acceptable range was achieved, the potentiodynamic test was ready to be conducted.

For each of the six braze alloys, eight samples were tested and a potentiodynamic polarization curve was produced. The potentiodynamic tests scanned ± 250 mV from the open circuit potential at a rate of 1 mV every six seconds. A 5 Hz bandpass filter was utilized within the software to decrease the noise from the current auto-ranging switching which had the possibility to miss data points without the filter. Finally, a Tafel regression was used to determine the corrosion potential of the braze alloy (Figure 10).

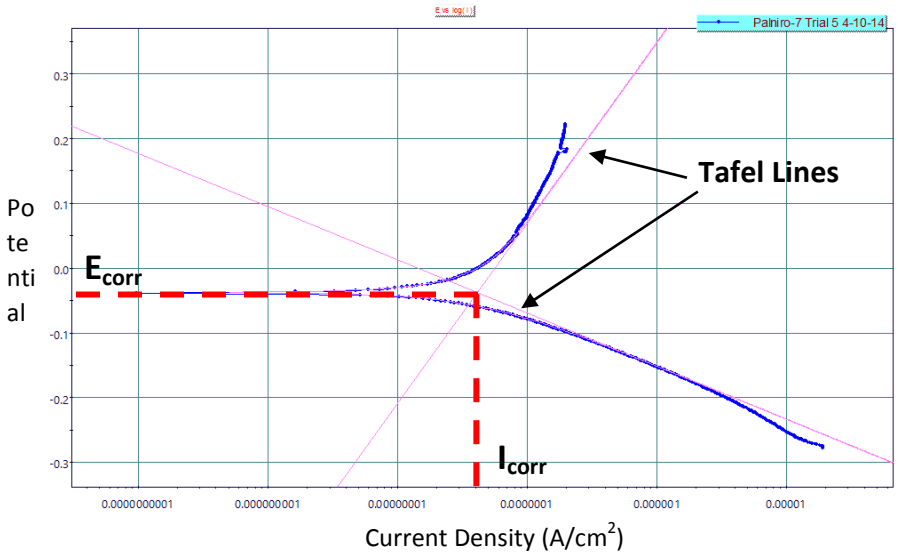

Figure 10. Potentiodynamic Polarization curve for a Palniro-7 sample. The voltage range is ± 250 mV from the open circuit potential at the beginning of the test. A Tafel approximation is shown with the resultant E_{corr} and I_{corr} values.

2.5 Statistical Analysis and Base Metal Comparison

JMP software was utilized to analyze the data produced through a variety of statistical measurements. Specifically, boxplots were used to show the overall spread of the data and 95% confidence/prediction intervals provided an indication of the range of potential values each alloy. These results were compared to the known electrochemical information of various industry-standard base alloys[18] to determine if each base-braze couple meets the ±250 mV specification. The results from each of these base-braze combinations were classified as either a "Pass", a "Failure", or a "Use with Caution" based on whether or not their confidence and prediction intervals were within ± 250 mV of the base metal's corrosion potential.

3. RESULTS

3.1 Potentiodynamic Polarization

The plot from Figure 10 is fairly representative of the shape of the curve for each of the six braze alloys although there were some notable differences in the upper, anodic region in a couple cases (Appendix A). However, in terms of scatter within each alloy type's eight trials, there were clear differences. For a visual depiction of the variance in the tests, each of the eight samples were superimposed on a single graph (Figure 11).

b) 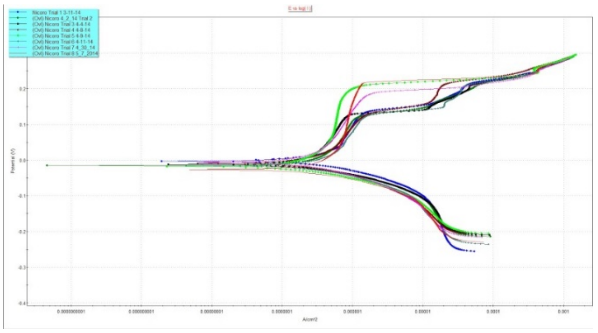 a) 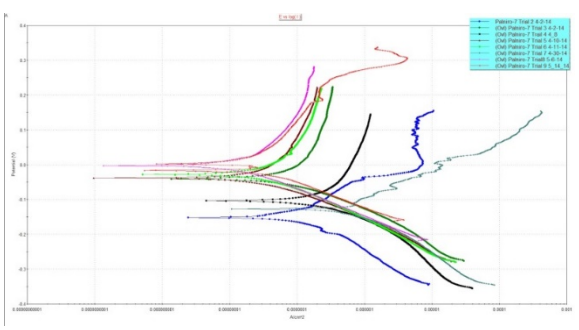

Figure 11. a) Eight potentiodynamic polarization curves for the Nicoro braze alloy. Around the corrosion potential value, there is nearly zero difference among the tests. b) Eight potentiodynamic polarization curves for the Palniro-7 braze alloy. This alloy showed the most scatter and there are clear discrepancies between the trials.

The corrosion potential for each sample is shown in Table III along with the range, standard deviation, and average corrosion potential for each alloy. Appendix A displays the potentiodynamic curves for each of the six braze alloys.

Table III: Ecorr Measurements of Wesgo Metals Braze Foil Samples

	Gold ABA	Nicoro®	Nioro®	Palniro-1®	Palniro-7®	Silver ABA
Trial Number	(V)	(V)	(V)	(V)	(V)	(V)
1	0.0306	-0.0023	-0.0113	0.0226	-0.1502	-0.1785
2	-0.0443	-0.0146	-0.0165	0.0748	-0.0406	-0.2084
3	-0.0595	-0.0110	-0.0718	-0.0158	-0.1038	-0.2040
4	-0.0699	-0.0081	-0.0313	0.0802	-0.0381	-0.2163
5	-0.1365	-0.0173	-0.0579	0.0126	-0.0281	-0.2114
6	-0.0566	-0.0158	-0.0779	-0.0180	-0.1266	-0.2162
7	-0.0425	-0.0054	-0.0554	-0.0432	-0.0037	-0.2115
8	0.0091	-0.0265	0.0094	0.0761	-0.0068	-0.1924
Range	167.10	24.14	87.26	123.38	146.58	37.78
Average	-0.0462	-0.0126	-0.0391	0.0237	-0.0622	-0.2048
Standard Deviation	0.0507	0.0076	0.0314	0.0485	0.0565	0.0131

Five out of the six braze alloys have average corrosion potentials between -0.062 mV and 0.024 mV, a 0.086 mV range. The other alloy, Silver ABA, was considerably more active with an average of -0.205 mV. There was a noticeable amount of spread between the standard deviation values for the alloys with the lowest at only 7.64 mV and the highest nearly an order of magnitude higher at 56.5 mV. The average standard deviation for all of the alloys was 34.6 mV. Similarly, there was a large spread in the data ranges for the individual alloys; in the worst case, Gold ABA had a range of 167.1 mV which spans a significant amount of the ± 250 mV guideline from the specification. In general, these differences indicate either some variance in the experimental procedure between tests or inherent differences in the electrochemical repeatability amongst the alloys themselves.

3.2 Statistical Analysis

The differences in the amount of variation between sample trials can be seen with a statistical box plot (Figure 12).

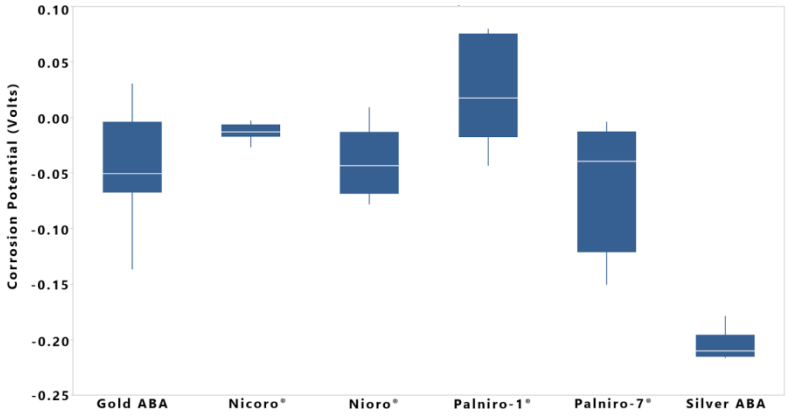

Figure 12. Box and whisker plots for each of the six braze alloys.

Each box plot shows the inherent range from the corrosion testing. It is of note that Silver ABA and Nicoro have the smallest scatter and the lowest concentration of gold alloying.

In addition to box plots, 95% confidence and prediction intervals were generated for all six braze alloys. For a visual indication of base-braze performance, these intervals were superimposed onto a box representing ± 250 mV from the base alloy's corrosion potential (Figure 13).

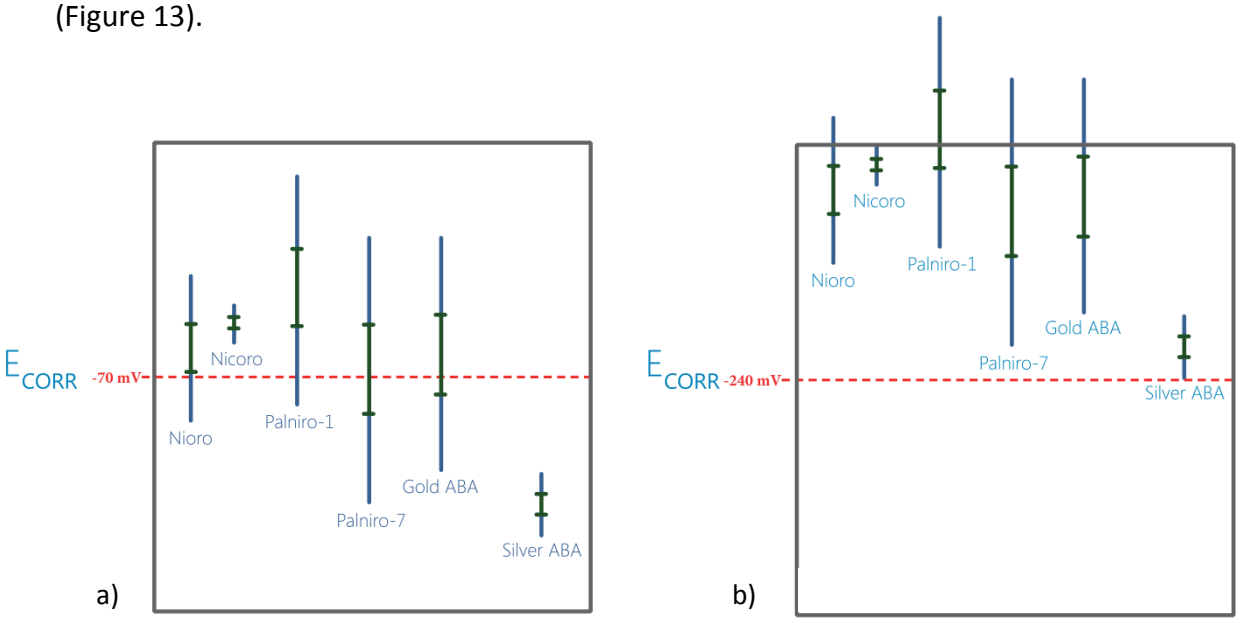

Figure 13. Base-braze comparison showing whether or not each braze alloy lies within the 500 mV range of a particular base metal. The green regions in the box represent the confidence intervals and the large blue lines represent the prediction intervals. a) Base metal A–286, a nickel-based superalloy. b) Base Metal Ti–6Al–4V.

Because all of the intervals lie within the box, it can be concluded that all alloys pass and are acceptable couples with A-286. In comparison, for the base metal Ti-6Al-4V, there are four different braze alloys with intervals which extend outside the blue box.

Completing this type of comparison for each of the base-braze couples enabled the development of a final recommendations table that serves as a guideline for Aerojet Rocketdyne in selecting galvanic couples for various applications (Table IV).

Table IV: Final Recommendations for Base-Braze Couples

	Inconel 718 (-290 mV)	Inconel 625 (-270 mV)	Inconel 600 (-280 mV)	A - 286 (-70 mV)	JBK - 75 (-70 mV)	347 SS (-80 mV)	304L SS (-100 mV)	Ti-6Al-4V (-240 mV)	Monel K-500 (-260 mV)	Monel 400 (-120 mV)	OFHC Copper (-160 mV)	C18200 (-170 mV)	Narloy-Z (-160 mV)
Nicoro® -12.63 mV± 7.64	277	257	267	57	57	67	87	227	247	107	147	157	147
Nioro® -39.07 mV± 31.37	251	231	241	31	31	41	61	201	221	81	121	131	121
Palniro-1® 23.66 mV± 48.46	314	294	304	94	94	104	124	264	284	144	184	194	184
Palniro-7® -62.2 mV ± 56.46	228	208	218	8	8	18	38	178	198	58	98	108	98
Gold ABA -46.18 mV± 50.57	244	224	234	24	24	34	54	194	214	74	114	124	114
Silver ABA -204.84 mV± 13.14	85	65	75	135	135	125	105	35	55	85	45	35	45

All Intervals Pass (43/72 = 59.7 %)

Prediction Interval Fails (11/72 = 15.3 %)

Confidence Interval Fails (18/72 = 25 %)

Listed across the top of the table are the base metals whose electrochemical potential values were obtained from the European Space Agency (ESA). On the left-hand side of the table, the braze alloys are listed with the average E_{corr} value found in this study. The color codes reflect a passing, failing, or use with caution rating (green, red, or orange, respectively). A failing rating meant that the confidence interval was outside of the ± 250 mV limit. If any part of the prediction interval was outside of the limit then a "use with caution" rating was selected. Approximately 60% of the alloy couples pass the ± 250 mV criteria, with the other 40% receiving either "use with caution", of "failing". Failing does not mean that the couple cannot be used, but that it may require galvanic protection to be used.

It is of note that this table used the confidence and prediction intervals as the main criteria for passing and failing, so although some cells may show values lower than 250 mV, this is not necessarily indicative of whether or not their intervals meet the specification.

4. DISCUSSION

4.1 Sources of Variation

When comparing the potentiodynamic polarization plots of the different alloys, it is clear that some exhibited more scatter between trials than others. In order to determine the reason for this difference in scatter and evaluate the degree of scatter in general, the procedural and environmental differences from test to test were analyzed. While every effort was made to follow the same procedure between tests and from each separate testing day to another, complete replication of experimental conditions was not always feasible. Of these conditions, the easiest to observe and interpret are those related to the procedures followed during sample preparation and testing processes. Before testing, each sample was cleaned in approximately the same amount of acetone for approximately the same amount of time. However, the depth that the acetone beaker was placed in the ultrasonic cleaning bath varied,

as well as the holding time in the acetone before the deionized water rinse and the holding time in the sample bag between rinsing and testing. The accumulation of these small variations in the cleaning procedure could potentially affect the overall surface cleanliness of each sample, leading to variability in the surface used for the testing. This surface variability when paired with the inconsistent room cleanliness of a non-cleanroom environment, could lead to the difference in values obtained from subsequent tests. In addition to the cleaning procedures showing signs of variation, the salt concentration in the electrolyte that was prepared for the electrochemical cell changed from test to test. When preparing the solution, 920 mL of water was added to a beaker with 34 grams of NaCl stirred in afterwards. Both of these values varied however, because the amount of water was measured in the beaker visually and the mass of salt added could only be measured to an accuracy of ± 1 mg. Based on differing salt concentrations, variation in the data would be expected.

When inspecting the procedures used to run the testing and to interpret the data, the equilibration period during which the open circuit voltage across the cell was monitored presented some deviations between different testing runs. While the practice of waiting for the V_{oc} drift to fall below 2-3 mV/min was used to decide when to start testing, some alloys did not have V_{oc} vs. Time plots that reached equilibrium within the time allotted. In these circumstances, the decision was made to either start the test or allow additional time for the system to reach equilibrium. However, the alloys that displayed this behavior generally did not show any improvement given additional equilibration time. Only three tests out of the 48 conducted experienced this problem, with two trials of the Gold ABA samples showing large V_{oc} drift, and one Nioro trial exhibiting a much higher V_{oc} than was shown by any other sample. By starting the test when the solution had potentially not yet reached equilibrium meant that the open circuit potential on which the scan range is based may not include the same amount of points in the cathodic and anodic regions. This circumstance is especially true of the Nioro sample because the higher-than-expected V_{oc} could have pushed the scan range out to the point that the transition from the cathodic to anodic region may have been lost. The exact effect of this difference is unknown but it could potentially lead to differences in the corrosion

potential found using the Tafel regression. In addition to V_{oc} drift affecting the Tafel fitting, the process of Tafel fitting itself offers variation. When selecting points to include in the regression performed by the software, the user manually encloses the portion of the plot used. Based on the slight variation in manually selecting points, the corrosion potential given by the software could be skewed from its true value.

In evaluating factors that were not controlled during testing, the temperature in the testing room and the dissolved oxygen concentration in the electrolyte could have changed the electrochemical measurements that were taken. First, fluctuations in temperature have been shown to cause large variations in electrochemical readings.[17] While the temperature in the testing room was believed to be the same throughout tests, data was not collected to prove this. Another factor that was not controlled was the dissolved oxygen content present in the electrolyte. Dissolved oxygen concentration refers to the amount of oxygen present in water separate from those in the actual water molecules. This extra oxygen in water enters from the atmosphere, and speeds up the rate at which metals corrode. This phenomenon takes place due to the interaction of the oxygen with hydrogen gas that is produced at the cathode of the electrochemical cell. The reaction between the two gasses causes depolarization and increases the corrosion of the metal. In this study, dissolved oxygen may have been introduced through the vigorous stirring of the salt into the distilled water, a processing step which likely differed in agitation speed and duration between tests. The varying level of dissolved oxygen content in the electrolyte can be ameliorated through the use of an inert gas purge through the system. By bubbling an inert gas through the electrolyte, the excess oxygen is removed from the system and the testing can be conducted without the dissolved oxygen effect.

In addition, the braze foils that were studied likely had a degree of inhomogeneity in their microstructures, which may have led to variations between samples. As stated by the company who supplied the foils, the chemical compositions of the alloys are tightly controlled but the cooling practices used in their fabrication are less closely monitored. From a non-equillibrium cooling, it is possible that different braze samples exhibited different microstructures and

possible higher localized concentrations of specific alloying elements. The differing microstructures resultant from these conditions could cause localized corrosion of the more active alloying elements and lead to an inaccurate corrosion potential measured for the braze sample.

In ASTM G59 it is stated that an average standard deviation of 3 mV between trials and 12 mV between labs is an acceptable amount of scatter in potentiodynamic polarization testing. Throughout our testing we found that we had an average standard deviation of approximately 35 mV. However, this specification tests 304 stainless steel samples in its study, which form a stable oxide and are believed the have a higher inherent repeatability of testing when compared with other alloys. Consequently, we attribute the main source of variation in our data to the composition of the alloy tested. Four of the six alloys tested have gold as the major alloying element, while the others are mainly comprised of copper and silver (Nicoro® and Palniro-7®, respectively). The four alloys with the most gold exhibited the largest scatter in their results. Due to the instability of the oxide formed on gold, it is believed to be more susceptible to external factors such as surface contamination and dissolved oxygen content in the electrolyte. In comparison to gold, silver and copper readily form more stable oxides, which leads to a lower amount of scatter in their data. This is confirmed by Nicoro® and Silver ABA both having the least amount of scatter and smallest ranges of the six alloys tested.

5. CONCLUSIONS

I. 60% of braze-base couples pass the 250 mV criteria for service.
II. 40% of couples should be evaluated for galvanic protection.
III. Variation seems to be associated with alloy composition. Alloys that form stable oxides (Nicoro and Silver ABA) exhibit less scatter than those with gold as the major alloying element.

6. REFERENCES

1. Sulzer Metco. An Introduction to Brazing: Fundamentals, Materials, Processing. Issue 3. August 2011.

2. Andersson, Rolf. “Brazing in Metals.” Linde Gas.

3. Jacobson, David M., and Giles Humpston. *Principles of Brazing*. Materials Park, NY: ASM International, 2005. Print.

4. “Braze Alloys Materials Selector”. Morgan Technical Ceramics. Morgan Crucible Company, 2009. Web. 19 Nov. 2013.

5. “Labeled Galvanic Cell.” Image. Wikipedia. Web. 4 January 2012.

6. R. Baboian, Galvanic Corrosion, Corrosion: Fundamentals, Testing, and Protection, Vol 13A, ASM Handbook, ASM International, 2003, p 210–213.

7. H.P. Hack, Evaluation Galvanic Corrosion, Corrosion: Fundamentals, Testing, and Protection, Vol 13A, ASM Handbook, ASM International, 2003, p 562–567.

8. ASTM Standard G082, 2004, “The Standard Guide of Development and Use of a Galvanic Series for Predicting Galvanic Corrosion Performance,” ASTM International, West Conshohocken, PA, 2004.

9. Thompson, Neil G., Joe H. Payer. “DC Electrochemical Test Methods”. NACE International. Volume 6. 1998. Houston, Texas.

10. Westerley. Chemical Corrosion. University of Rhode Island. n.d. Web. Nov. 2013.

11. S.C. Dexter, Corrosion in Seawater, Corrosion: Environments and Industries, Vol 13C, ASM Handbook, ASM International, 2006, p 27–41.

12. “Liquid Rocket Engine Nozzles.” Boeing Rocketdyne. http://www.docstoc.com/docs/51976123/Liquid-Rocket-Engine-Nozzles

13. Sandin, Tom. “Aerospace Brazing Today & Tomorrow”. Welding Design & Fabrication. Feb. 7, 2013.

14. Schennach, Robert. “Electrochemical Kinetics of Corrosion”. Graz University of Technology.

15. Polarization Diagram of a Passivable System. NACE International, 2010. http://events.nace.org/library/corrosion/AnodProtect/passivecurve.asp

16. ASTM Standard G61, 2014, “Standard Test Method for Conducting Cyclic Potentiodynamic Polarization Measurements for Localized Corrosion Susceptibility of Iron-, Nickel-, or Cobalt-Based Alloys,” ASTM International, West Conshohocken, PA, 2014.

17. Sheridan, Leah. Princeton Applied Research. (Personal Communication March 11, 2014).

18. “Electromotive Force of Metals and Alloys.” European Space Agency. June 4, 2014. ESMAThttp://esmat.esa.int/Services/bimetallic_data/Bimetaltable/bimetalemf.html

Appendix A

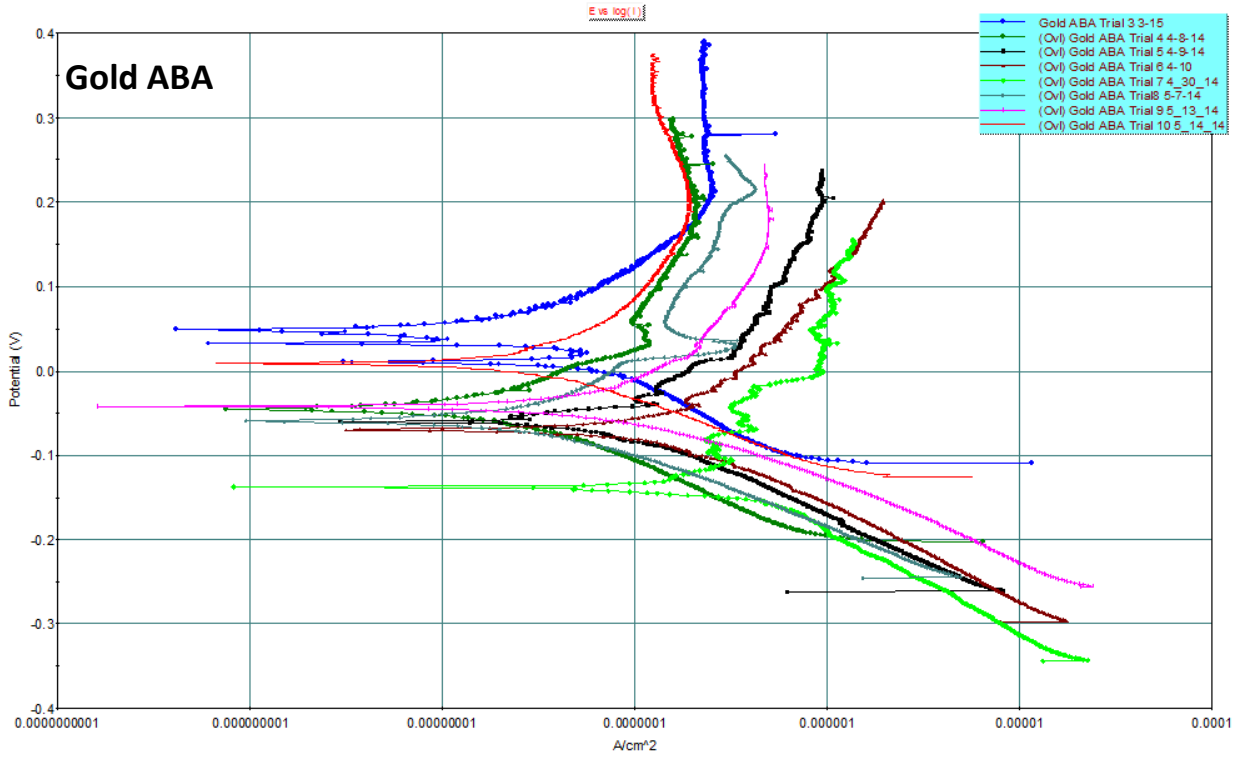
E vs. log(I)
Gold ABA
Gold ABA Trial 3 3-15
(Ovl) Gold ABA Trial 4 4-8-14
(Ovl) Gold ABA Trial 5 4-9-14
(Ovl) Gold ABA Trial 6 4-10
(Ovl) Gold ABA Trial 7 4_30_14
(Ovl) Gold ABA Trial8 5-7-14
(Ovl) Gold ABA Trial 9 5_13_14
(Ovl) Gold ABA Trial 10 5_14_14
Potential (V)
0.4
0.3
0.2
0.1
0.0
-0.1
-0.2
-0.3
-0.4
0.0000000001
0.000000001
0.00000001
0.0000001
0.000001
0.00001
0.0001
A/cm^2

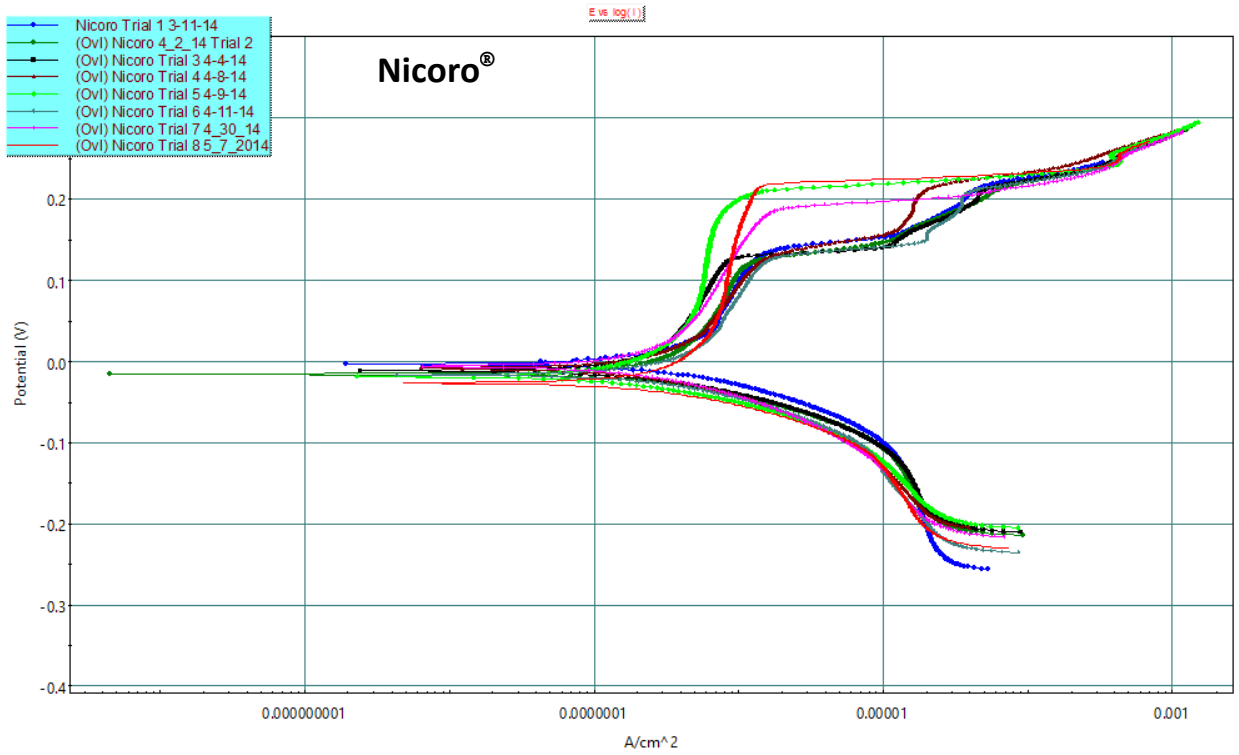
E vs. log(I)
Nicoro®
Nicoro Trial 1 3-11-14
(Ovl) Nicoro 4_2_14 Trial 2
(Ovl) Nicoro Trial 3 4-4-14
(Ovl) Nicoro Trial 4 4-8-14
(Ovl) Nicoro Trial 5 4-9-14
(Ovl) Nicoro Trial 6 4-11-14
(Ovl) Nicoro Trial 7 4_30_14
(Ovl) Nicoro Trial 8 5_7_2014
Potential (V)
0.2
0.1
0.0
-0.1
-0.2
-0.3
-0.4
0.000000001
0.0000001
0.00001
0.001
A/cm^2

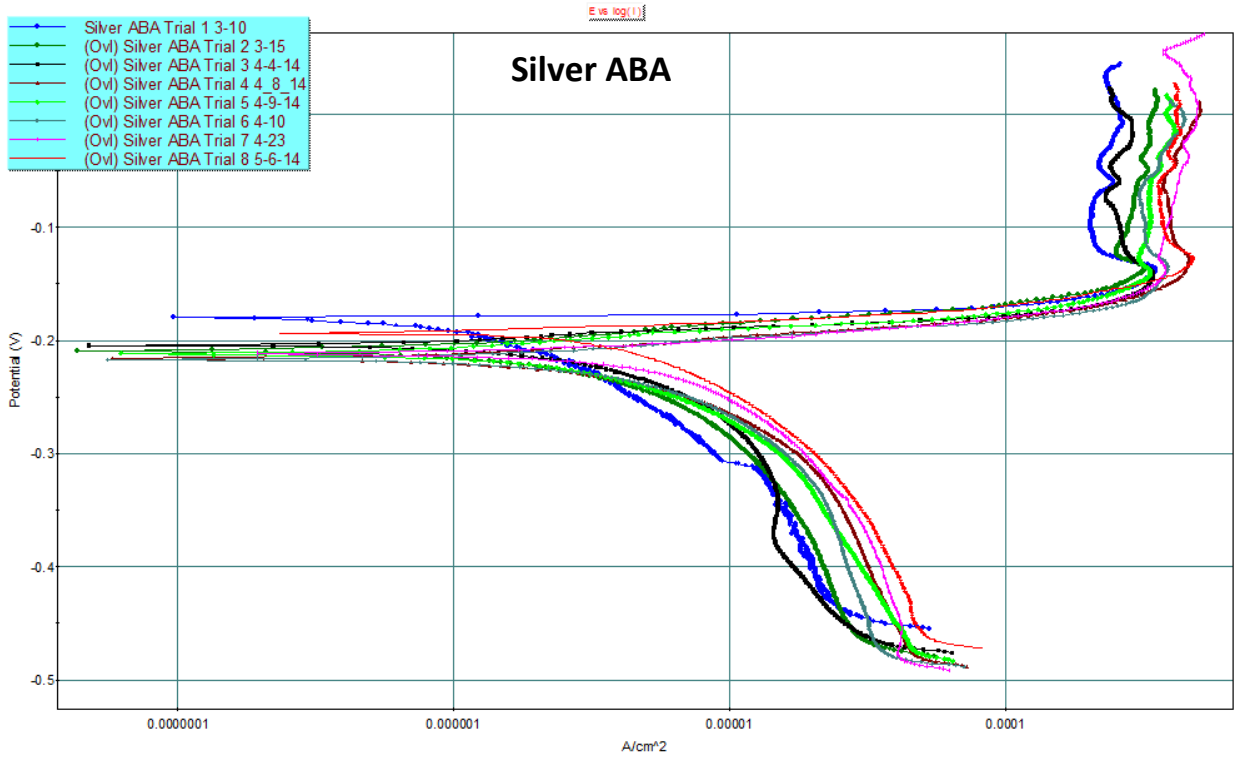
Silver ABA
Silver ABA Trial 1 3-10
(Ovl) Silver ABA Trial 2 3-15
(Ovl) Silver ABA Trial 3 4-4-14
(Ovl) Silver ABA Trial 4 4_8_14
(Ovl) Silver ABA Trial 5 4-9-14
(Ovl) Silver ABA Trial 6 4-10
(Ovl) Silver ABA Trial 7 4-23
(Ovl) Silver ABA Trial 8 5-6-14
Potential (V)
-0.1
-0.2
-0.3
-0.4
-0.5
0.0000001
0.000001
0.00001
0.0001
A/cm^2

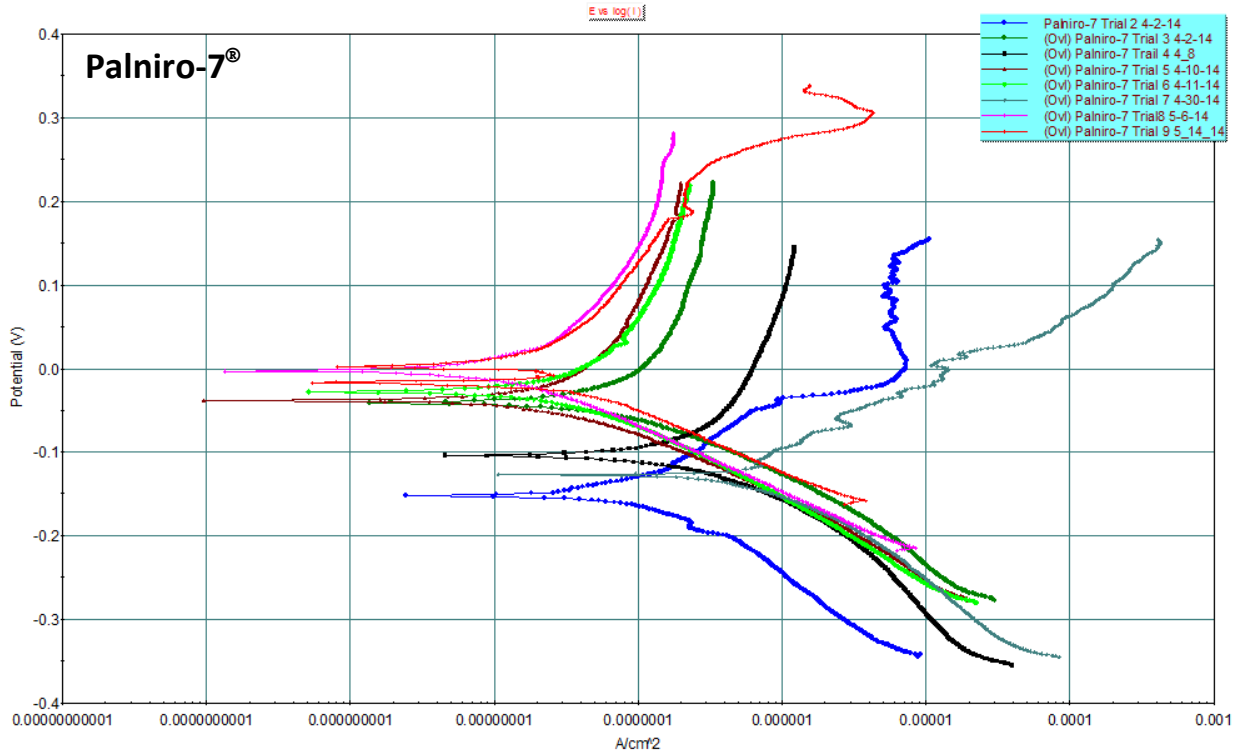
Palniro-7®
Palniro-7 Trial 2 4-2-14
(Ovl) Palniro-7 Trial 3 4-2-14
(Ovl) Palniro-7 Trail 4 4_8
(Ovl) Palniro-7 Trial 5 4-10-14
(Ovl) Palniro-7 Trial 6 4-11-14
(Ovl) Palniro-7 Trial 7 4-30-14
(Ovl) Palniro-7 Trial8 5-6-14
(Ovl) Palniro-7 Trial 9 5_14_14
Potential (V)
0.4
0.3
0.2
0.1
0.0
-0.1
-0.2
-0.3
-0.4
0.00000000001
0.0000000001
0.000000001
0.00000001
0.0000001
0.000001
0.00001
0.0001
0.001
A/cm^2

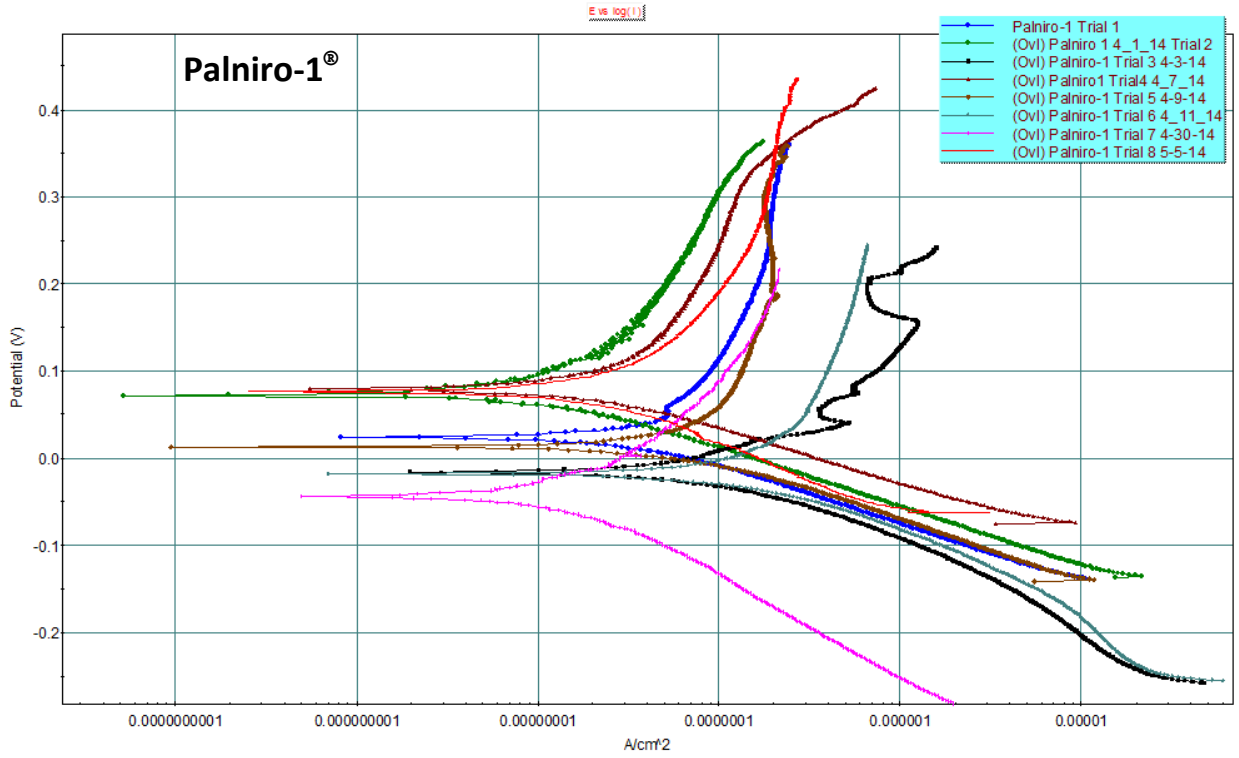
Palniro-1®
E vs. log(I)
Palniro-1 Trial 1
(Ovl) Palniro 1 4_1_14 Trial 2
(Ovl) Palniro-1 Trial 3 4-3-14
(Ovl) Palniro1 Trial4 4_7_14
(Ovl) Palniro-1 Trial 5 4-9-14
(Ovl) Palniro-1 Trial 6 4_11_14
(Ovl) Palniro-1 Trial 7 4-30-14
(Ovl) Palniro-1 Trial 8 5-5-14
Potential (V)
0.4
0.3
0.2
0.1
0.0
-0.1
-0.2
0.0000000001
0.000000001
0.00000001
0.0000001
0.000001
0.00001
A/cm^2

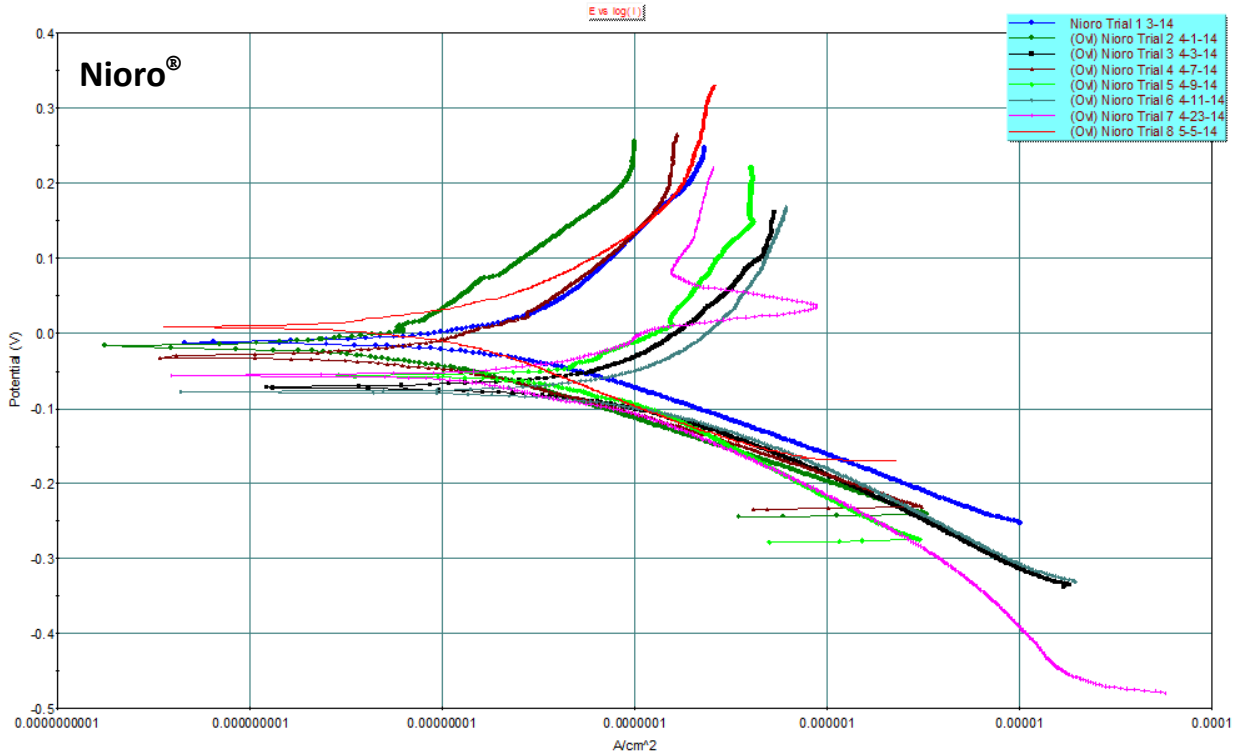
Nioro®
E vs. log(I)
Nioro Trial 1 3-14
(Ovl) Nioro Trial 2 4-1-14
(Ovl) Nioro Trial 3 4-3-14
(Ovl) Nioro Trial 4 4-7-14
(Ovl) Nioro Trial 5 4-9-14
(Ovl) Nioro Trial 6 4-11-14
(Ovl) Nioro Trial 7 4-23-14
(Ovl) Nioro Trial 8 5-5-14
Potential (V)
0.4
0.3
0.2
0.1
0.0
-0.1
-0.2
-0.3
-0.4
-0.5
0.0000000001
0.000000001
0.00000001
0.0000001
0.000001
0.00001
0.0001
A/cm^2

Appendix B

2014

Standard Operating Procedure for Potentiodynamic Polarization tests using the PARSTAT 2273

Max Martin
Mason Morgan
Matt Vance

Cal Poly
Materials Engineering

Testing Flowchart

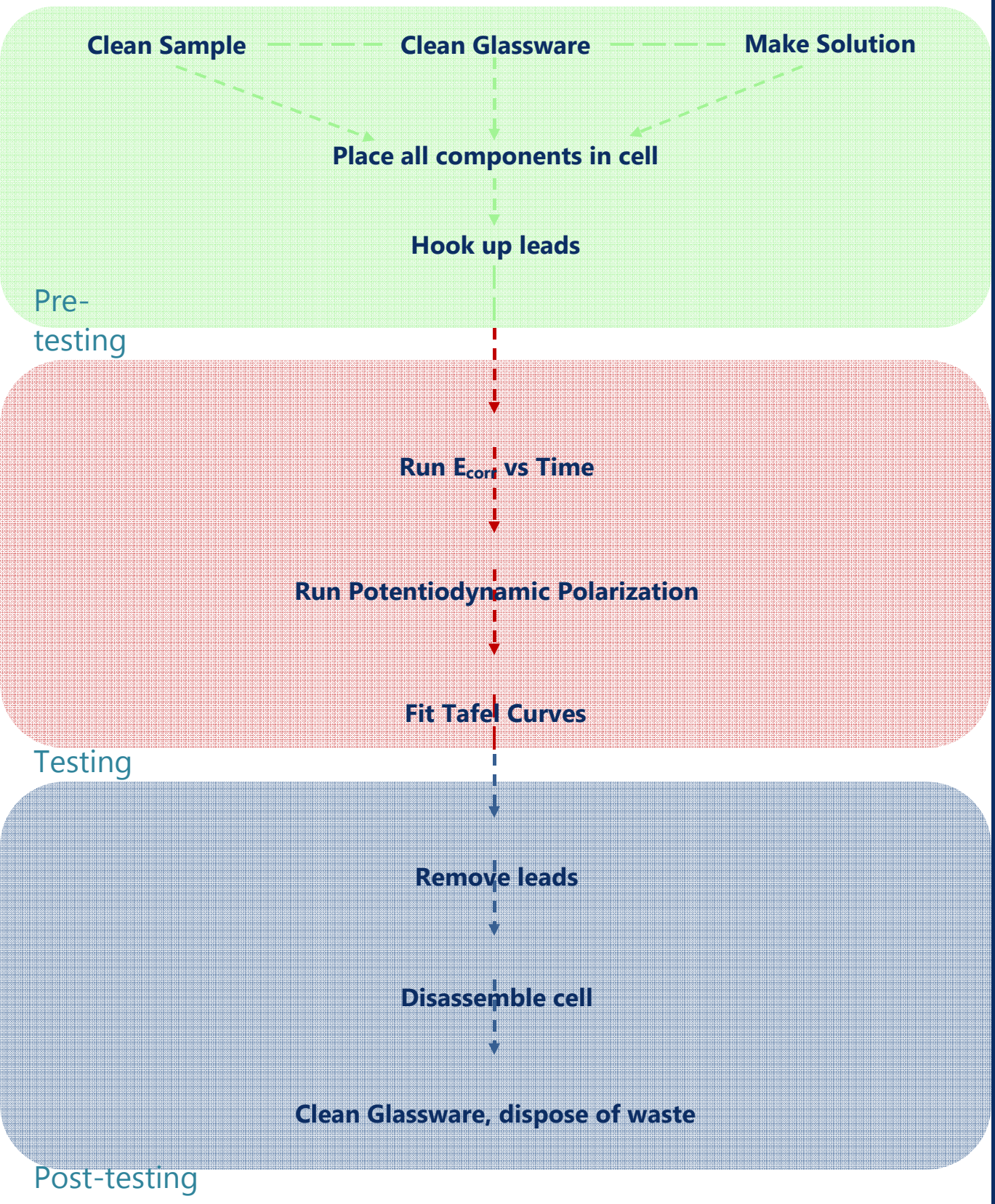

Parts List

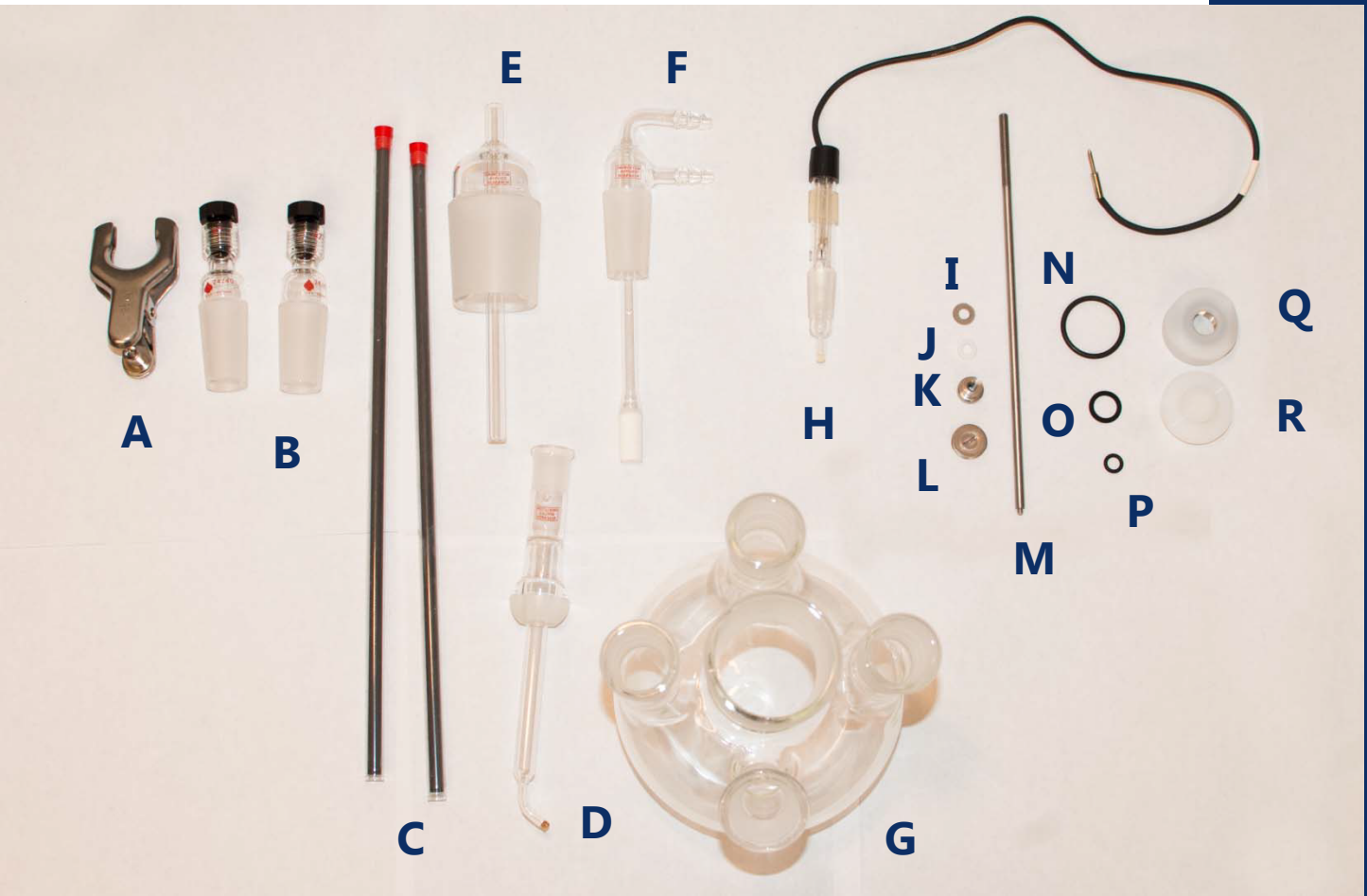

A. Ball and Socket Clamp
B. Glass Counter Electrode Adapters
C. Graphite Rods
D. Reference Electrode Bridge Tube
E. Sample Holder
F. Gas In / Out Adapter
G. Corrosion Round Bottom Flask
H. Saturated Calomel Reference Electrode
I. Flat Stainless Steel Washer
J. Flat Teflon Washer
K. Knurled Thumb Nut
L. Sample Holder Plug (Flat Cell)
M. Sample Holder Rod (Flat Cell)
N. Kalrez O-Rings (Flat Cell)
O. Kalrez Flat Washer
P. Small Flat Cell O-Ring
Q. Sample Holder Body (Flat Cell)
R. Sample Holder Cap (Flat Cell)

Sample Preparation

Step 1: For detailed cleaning instructions refer to ASTM G5.

Step 2: Place test sample in a clean beaker filled with acetone.

Step 3: Using an ultrasonic bath, place the beaker in the solution for at least 2.5 minutes. (Turn the knob past “5” on the timer)

Step 4: Using tweezers that will not react with the acetone, remove the sample from the beaker, rinse thoroughly with DI water and dry using an inert gas.

Step 5: Place the cleaned sample in a sanitary container for transport to the testing apparatus.

Making the 3.5% NaCl solution

Step 1: Weigh 34.0 g of salt (+/- 0.01 g)—we used Morton's non-iodized
Step 2: Pour 920 mL of distilled water into a clean beaker
Step 3: Add the salt to the water and stir vigorously

NOTE: Solution should be prepared and used in one day—allowing the solution to sit for extended periods of time (multiple days) may affect the data

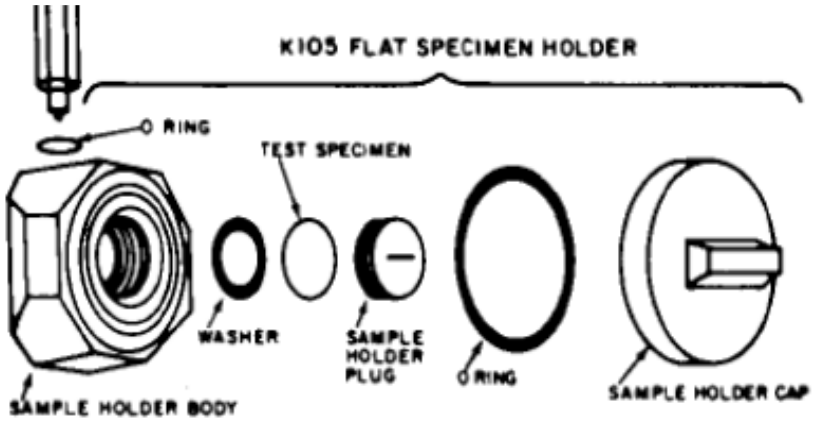

Step 1: Place Kalrez flat washer **(O)** inside the sample holder body **(Q)**.
Step 2: Place the cleaned flat sample into the sample holder body (on top of the washer). Be sure that the sample lies flat before continuing.
Step 3: Screw the sample holder plug **(L)** into the body with a flat-head screwdriver. This plug should be tightened so that the sample is secured in place (shake to be sure no motion is heard).
Step 4: Place the Kalrez O-Ring **(N)** into the groove on the holder body. **Step 5:** Screw the sample holder cap **(R)** onto the holder body. Tighten it by hand so that no solution will be able to get inside the holder.
Step 6: Place the small flat cell O-Ring **(P)** into the threaded hole on the holder body.

NOTE: See Princeton Applied Research Flat Cell literature for more detailed instructions

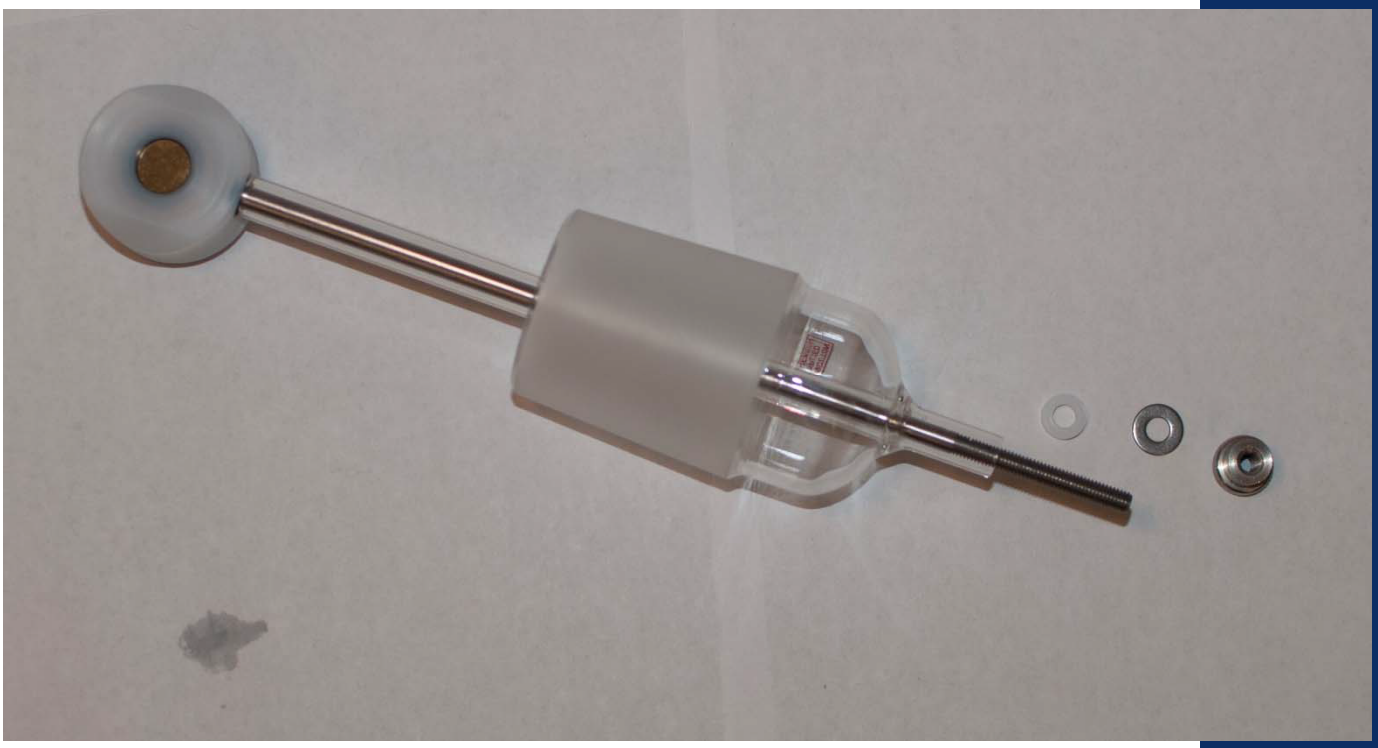

Step 1: Take the end of the sample holder rod **(M)** with less threading and attach it to the flat cell holder.
Step 2: Put the other end of the sample holder rod through the sample holder **(E)**.
Step 3: Place the flat Teflon washer **(J)**, the flat SS washer **(I)**, and the knurled thumb nut **(K)** onto the threaded end of the sample holder rod. Secure the flat sample holder by tightening the knurled nut.

Reference Electrode Setup

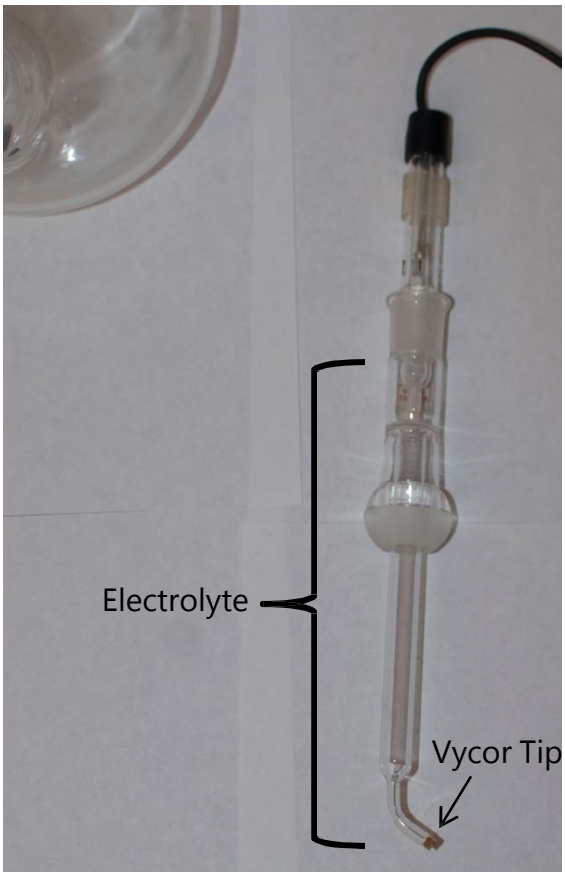

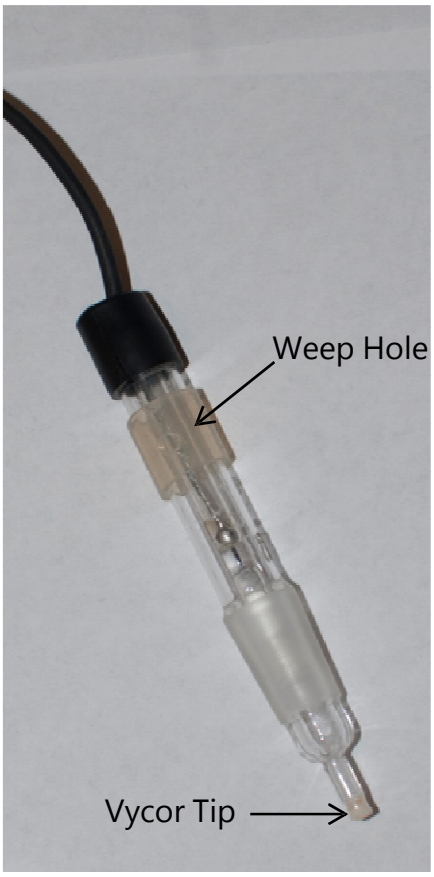

Step 1: Fill the reference bridge tube **(D)** with the electrolyte solution (3.5% NaCl for our tests).

Step 2: Expose the "weep hole" on the reference electrode **(H)** (Standard Calomel Electrode for us). Do this by moving the rubber sheath down so that the hole in the glass is no longer covered.

Step 3: Place the reference electrode **(H)** into the bridge tube **(D)**, making sure that the tip of the electrode is immersed in the solution of the bridge tube.

NOTE: When the reference electrode and the reference bridge tube are not in use, they should be stored in an electrolyte solution (3.5% NaCl for us). If the Vycor tips are allowed to dry out (~5 minutes after being wet) they can crack and will need replacement. If you are using an electrolyte other than NaCl, be sure to read ASTM standards to determine the proper storage solution for the reference electrode.

Installing Counter Electrodes

Step 1: Put nitrile gloves on to avoid contaminating the electrodes.
Step 2: Place the two glass counter electrode adapters **(B)** into the flask.
Step 3: Place an O-ring over each graphite rod **(C)** (around 1/3 of the way).
Step 4: Put the rods in the adapters (should go into solution but not touch the edges of the flask wall).

Step X: Adjust the reference electrode bridge tube to make sure the tip is roughly twice the tip diameter away from the surface of the sample, use the clamp to secure the tube.

Step X: The installed Ball and Socket Clamp (A).

Full Cell Assembly

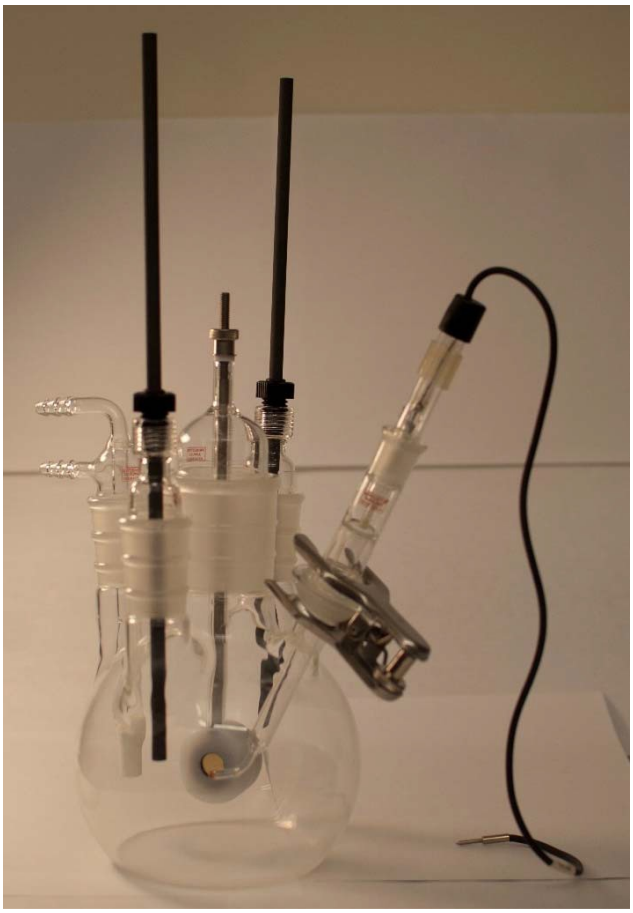

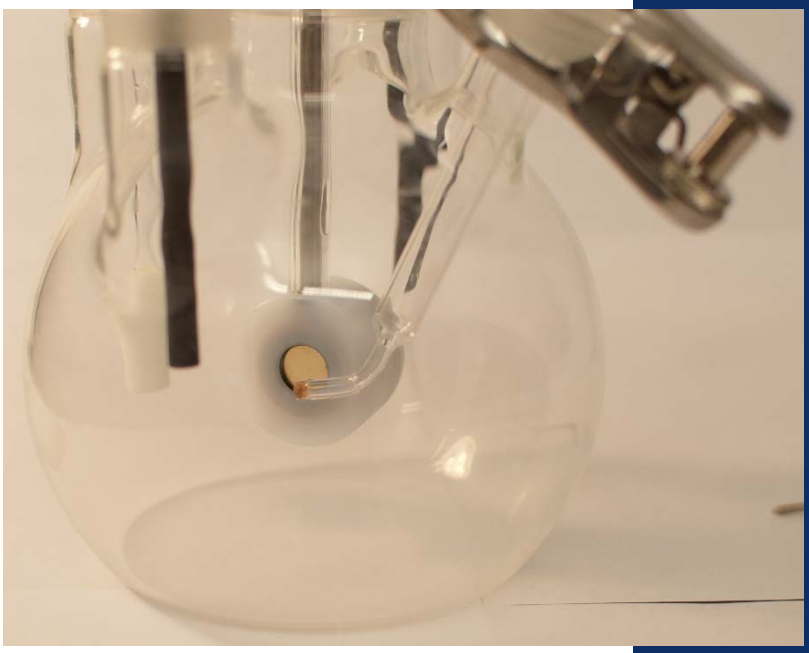

Step 1: Pour the electrolyte solution into the cell flask **(G)**.
Step 2: Place the graphite rods and their adapters **(C, B)** into the flask.
Step 3: Place the gas in/out adapter **(F)** into the flask.
Step 4: Put the assembled working electrode holder in the flask.
Step 5: Place the reference electrode in the cell, use the ball and socket clamp **(A)** to hold the tip of the bridge tube **(D)** approximately two times its own diameter away from the sample face.

NOTE: The tip of the bridge tube seen on the picture on the right is brown because it has dried out. Your Vycor tip should appear white.

Connecting Leads to the Cell

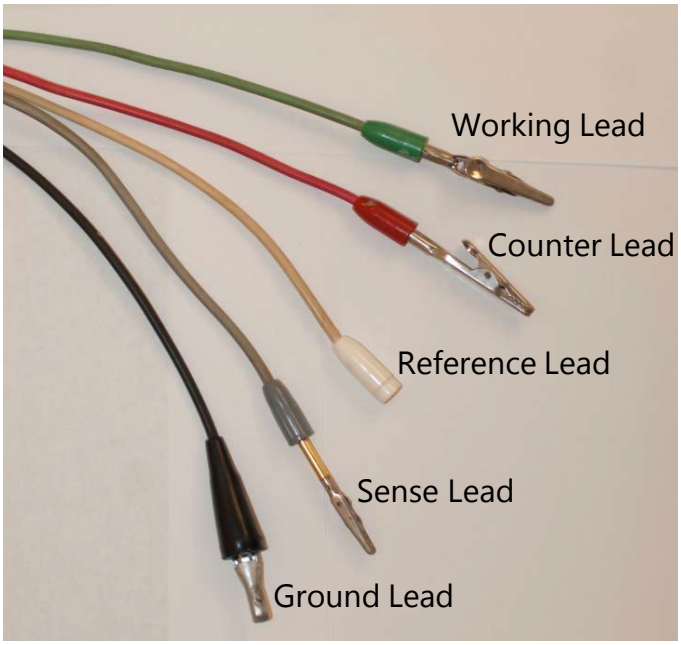

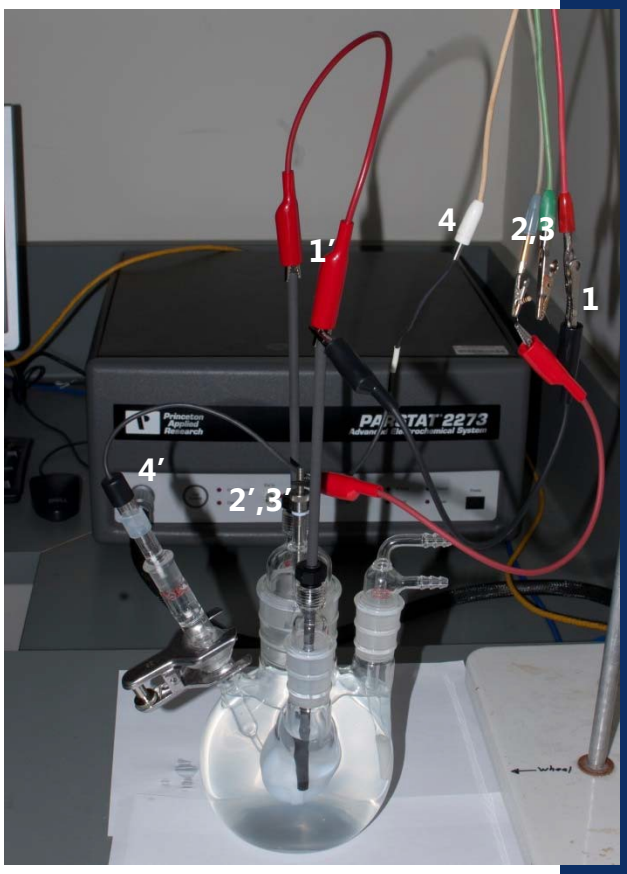

Step 1: Bridge the two graphite electrodes using an alligator clip
Step 2: Attach the red lead (counter) from the potentiostat **(1)** to one of the alligator clips on a graphite electrode **(1')** (may require another alligator clip depending on setup).
Step 3: Attach both the green working lead **(2)** and the gray sense lead **(3)** to the working electrode holder **(2', 3')**.
Step 4: Insert the pin from the reference electrode **(4')** into the white reference lead **(4)** from the potentiostat.
Step 5: Make sure the black ground lead is not attached to anything.

NOTE: Make sure none of the leads are intertwined or touch each other.

*If you see too much noise in the data, a resistor can be added between the working and sense leads (See right).

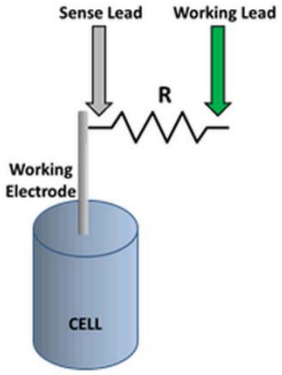

PowerCorr Software – Button Bar

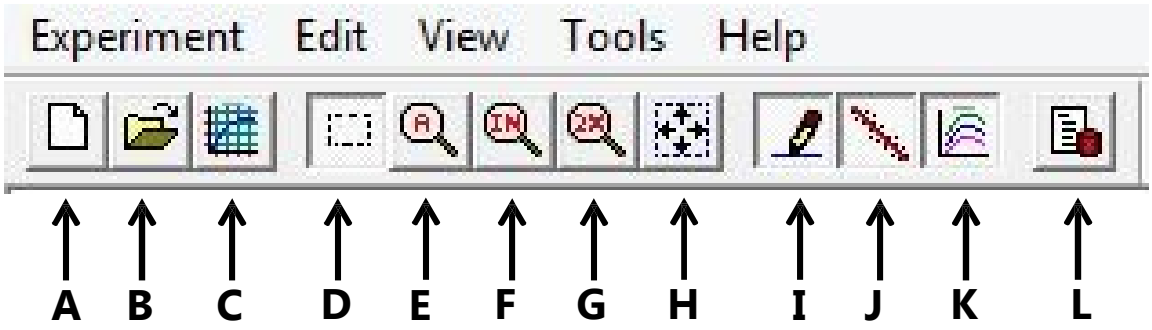

A. New Experiment
B. Open Experiment
C. New Graph
D. Selection Tool (Pick Individual Points or Draw Selection Box)
E. Autoscale Entire Graph
F. Zoom In (Draw Selection Box)
G. Zoom Out, 2X
H. Data Move / Pan Tool
I. View User Lines Toggle
J. View Analysis (Tafel Fits…) Toggle
K. View Overlays Toggle
L. Experimental Properties

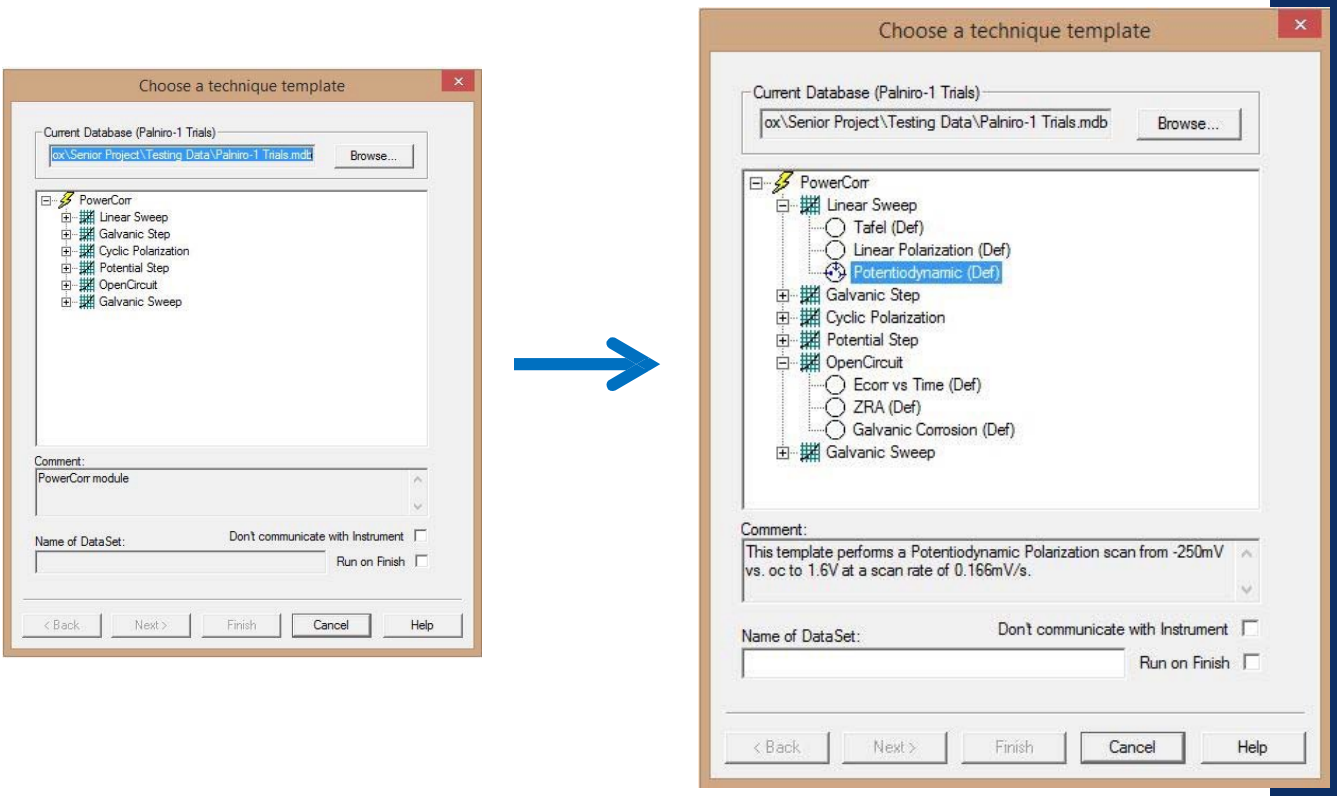

Step 1: Press the New Experiment button on the tool bar or select 'New Experiment' under the File pull down menu bar.

Step 2: In the experiment dialogue click on the '+' symbol on the left of the experiment type desired to expand the selection. Multiple sections can be expanded at the same time

Step 3: Selecting an experiment type lists a brief template of parameters in the comments section of the dialogue.

Step 4: Type in a name for the experiment and then click next to open the 'Cell Definition Window'.

PowerCorr Software – Cell Definition Window

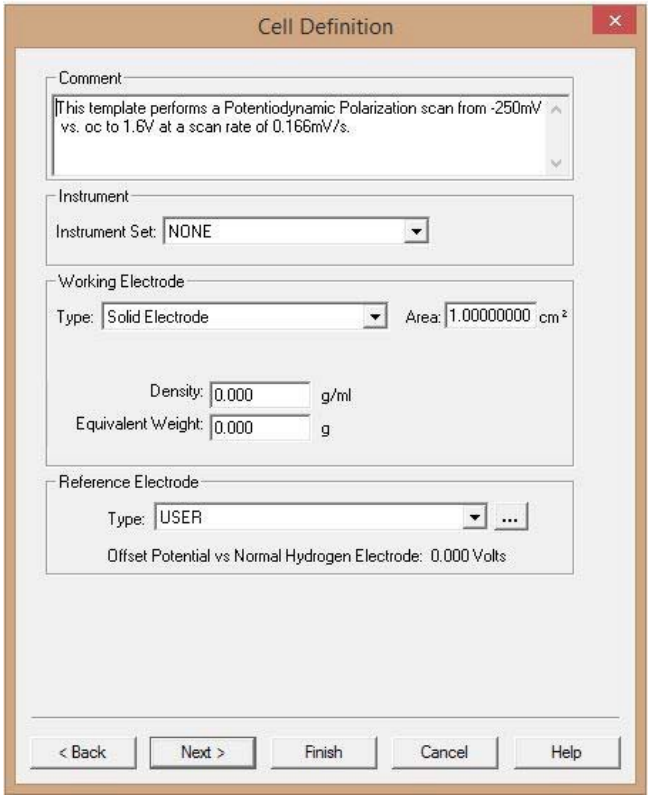

Step 1: Under the working electrode pull down menu select the type of electrode being used. (Typically Solid Electrode is used)

Step 2: Type in the area of the sample exposed to the testing solution. If using a flat cell the number will be 1 cm^2.

Step 3: Fill in the alloy density field.

Step 4: The equivalent weight needs to be calculated using the molar mass of the alloy and the stable charge of the dissociated ion. A rule of mixtures is used to account for the various compositions.

Table I: Ex Calculation, Gold ABA

Composition	**Atomic Weight**	**Stable Charge**	**Equivalent Weight***	**% Equivalent Weight****
96.4% Au	196.96 g	+3	65.655 g	63.291 g
3.0 % Ni	58.693 g	+2	29.347 g	0.8804 g
.6% Ti	47.867 g	+4	11.967 g	0.0718 g
		Total Alloy Equivalent Weight:		64.244 g

*(Atomic Weight * Stable Charge)

** (Equivalent Weight * Composition

Step 5: Using the pull down menu select the type of Reference electrode being used, the list also includes the standard potential offset from the SHE (standard hydrogen electrode).

Step 6: Click "Next" to move on to the Scan Definition Dialogue

PowerCorr Software – Scan Definition

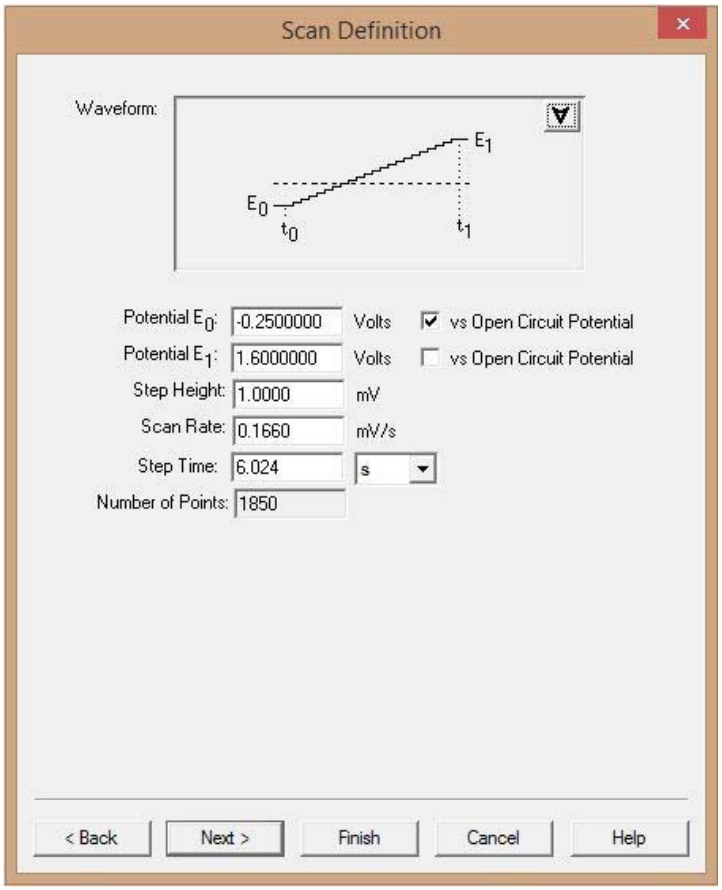

Step 1: Fill in the Potential E_0 field, and check the "vs Open Circuit Potential" box. This tells the program where to start testing.

Step 2: Fill in the Potential E_1 field, and check the "vs Open Circuit Potential" box. This tells the program where to end the test.

Step 3: Choose a step height for the program to determine what increments the measuremetns will be taken.

Step 4: Deciding on a scan rate tells the program how quickly to change the potential during the scan.

Step 5: The step time field determines how long the program holds at a specific voltage before moving up a step. This should be automatically calculated based on the Scan Rate and Step Height.

Step 6: Click Next to move onto the Pre Scan Definition dialogue.

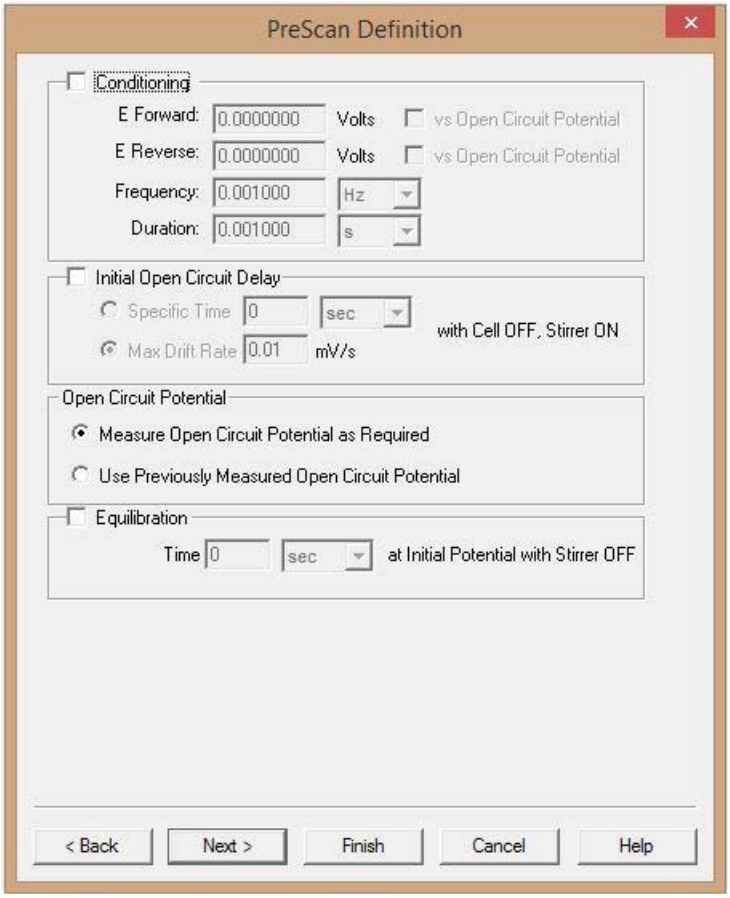

Step 1: Most settings on this dialogue can be left set as default.

Step 2: If desired check the "Initial Open Circuit Delay" box and select a time period for the software to hold before starting to run the experiment. Or, select a maximum drift rate for the software to monitor before beginning to run the experiment.

Step 3: Click Next to proceed to the last dialogue window; Expert Options.

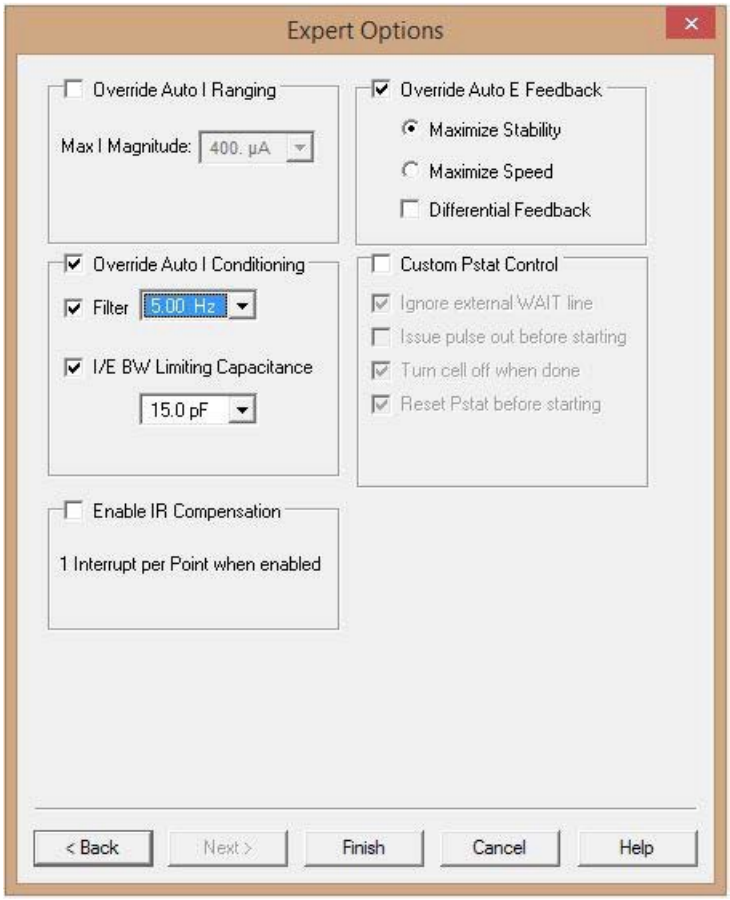

Step 1: In order to generate cleaner data the expert options window can be used to add additional settings into the system.
Step 2: Check the "Override Auto I Conditioning"
Step 3: Check the "Filter" box and select the desired filter to be applied from the pull down menu. Start with the slowest filter (5Hz) and increase as necessary.
Step 4: Check "I/E BW Limiting Capacitance" and if possible select a capacitance value from the pull down menu.
Step 5: Click finish to complete the experiment setup. Make sure the ParStat machine is turned on prior to hitting finish in order for a proper boot up sequence to occur.

Running a Test

Step 1: Press the Play button to begin the test (make sure that the 'Cell Enabled' button is pressed on the potentiostat).

Step 2: When prompted select the "Use External Cell" toggle and click OK.

Step 3: To end a test prematurely click on the Stop square on the test panel.

Step 4: (1) and (2) indicate a live feed of current and voltage outputs being monitored from the ParStat.

PowerCorr Software- Adding a Tafel Fit

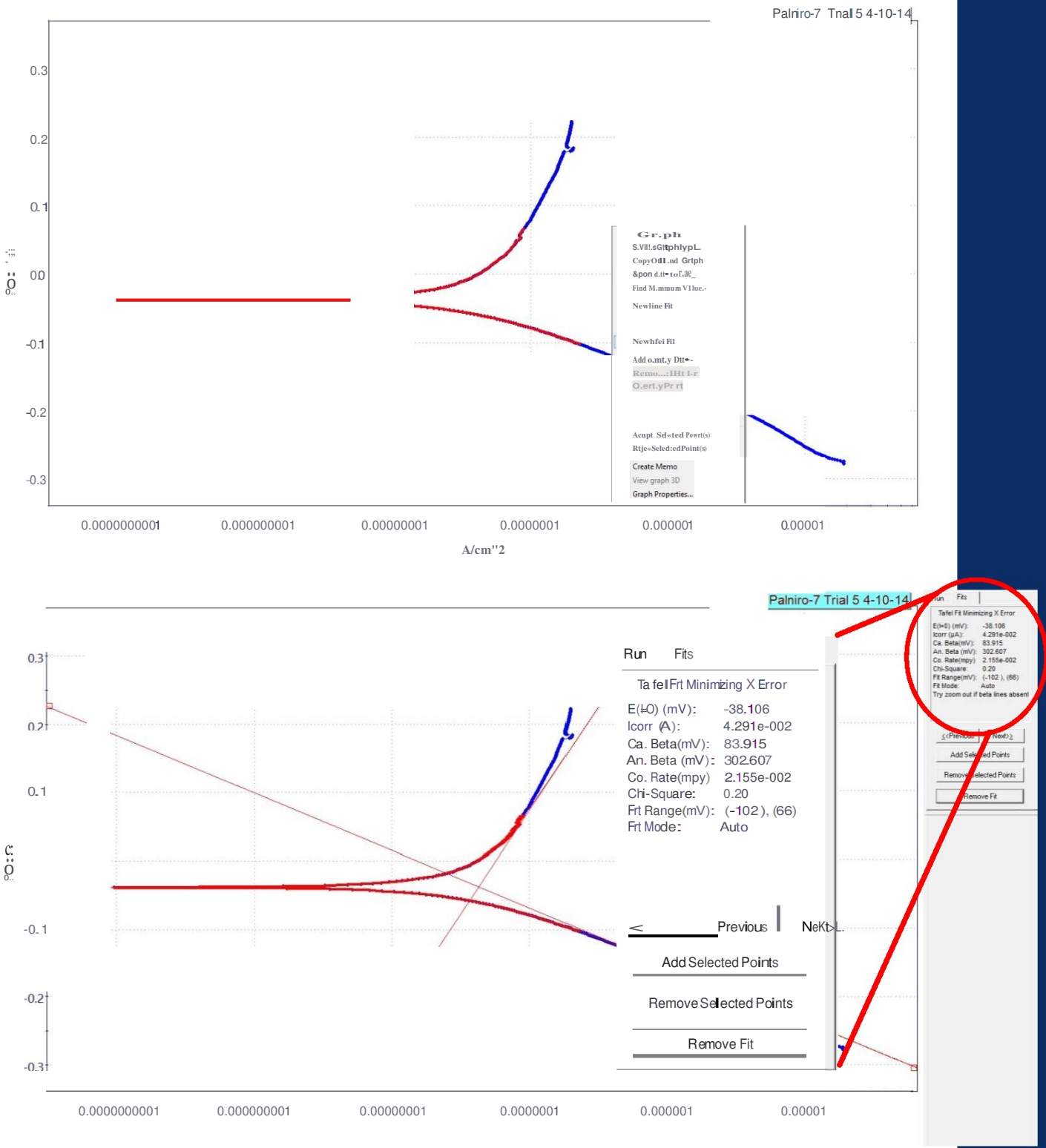

Step 1: Under graph properties, uncheck the Normalize with Area box.

Step 2: Highlight the data range using the 'Select Data Points' tool. The Tafel fit will only apply to the region of data points selected.

Step 3: Right click on the graph and select 'New Tafel Fit'.

Useful Resources

Standards

1) ASTM G5 – Standard Reference Test Method for Making Potentiodynamic Anodic Polarization Measurements
2) ASTM G59 – Standard Test Method for Conducting Potentiodynamic Polarization Resistance Measurements
3) ASTM G69 – Standard Test Method for Measurement of Corrosion Potentials of Aluminum Alloys
4) ASTM G71 – Standard Guide for Conducting and Evaluating Corrosion Tests in Electrolytes
5) ASTM G102 – Standard Practice for Calculation of Corrosion Rates and Related Information from Electrochemical Measurements

Books

1) ASM Handbook
    a. Sections on galvanic corrosion
2) DC Electrochemical Test Methods – Thompson & Payer
    a. Dr. London or Professor Gibbs should have this
3) Corrosion Tests and Standards: Application and Interpretation – Baboian
    a. You should be able to find this on Google Books

People

1) Dr. Walsh
2) Professor Gibbs
3) Leah Sheridan from Princeton Applied Research